Heliyon 10 (2024) e37147

Contents lists available at ScienceDirect

Heliyon

journal homepage: www.cell.com/heliyon

Research article

Bis-chalcones obtained *via* one-pot synthesis as the anti-neurodegenerative agents and their effect on the HT-22 cell line

Dorota Olender [a,*], Jacek Kujawski [a], Bartosz Skóra [b], Ewa Baranowska-Wójcik [c], Katarzyna Sowa-Kasprzak [a], Anna Pawełczyk [a], Lucjusz Zaprutko [a], Dominik Szwajgier [c], Konrad A. Szychowski [b]

[a] *Chair and Department of Organic Chemistry, Faculty of Pharmacy, Poznan University of Medical Sciences, Rokietnicka 3, 60-806, Poznań, Poland*
[b] *Department of Biotechnology and Cell Biology, Medical College, University of Information Technology and Management in Rzeszow, Sucharskiego 2, 35-225, Rzeszów, Poland*
[c] *Department of Biotechnology, Microbiology and Human Nutrition, University of Life Sciences in Lublin, Skromna 8, 20-704, Lublin, Poland*

ARTICLE INFO

Keywords:
Bis-chalcones
Claisen-Schmidt reaction
Anti-neurodegenerative activity
Cytotoxicity
Molecular docking

ABSTRACT

In the area of research on neurodegenerative diseases, the current challenge is to search for appropriate research methods that would detect these diseases at the earliest possible stage, but also new active structures that would reduce the rate of the disease progression and minimize the intensity of their symptoms experienced by the patient. The chalcones are considered in the context of candidates for new drugs dedicated to the fight against neurodegenerative diseases. The synthesis of *bis*-chalcone derivatives **(3a-3d),** as aim molecules was performed. Their structures were established by applying ^{1}H NMR, ^{13}C NMR, MS, FT-IR and UV–Vis spectra. All *bis*-chalcones were synthesized from terephthalaldehyde and appropriate aromatic ketone as substrates in the Claisen-Schmidt condensation method and evaluated in the biological tests and *in silico* analysis. Compounds exerted antioxidant activity using the HORAC method (**3a-3d**) and decreased the activities of GPx, COX-2 (**3b-3d),** GR (**3a-3c**) and CAT (**3a,3b)**. The high anti-neurodegenerative potential of all four *bis*-chalcones was observed by inhibition of acetyl- (AChE) and butyrylcholinesterase (BChE) and a positive effect on the mouse hippocampal neuronal HT-22 cell line (LDH release and PGC-1α, PPARγ and GAPDH protein expression). TD-DFT method (computing a number of descriptors associated with HOMO–LUMO electron transition: electronegativity, chemical hardness and potential, first ionization potential, electron affinity) was employed to study the spectroscopic properties. This method showed that the first excited state of compounds was consistent with their maximum absorption in the computed UV–Vis spectra, which showed good agreement with the experimental spectrum using PBE1PBE functional. Using *in silico* approach, interactions of *bis*-chalcones with selected targets (aryl hydrocarbon receptor (AhR) PAS-A Domain, ligand binding domain of human PPAR-γ, soman-aged human BChE-butyrylthiocholine complex, *Torpedo californica* AChE:N-piperidinopropyl-galanthamine complex and the COX-2-celecoxib complex) were characterized. Results obtained in *in silico* models were consistent with *in vitro* experiments.

* Corresponding author.
E-mail address: dolender@ump.edu.pl (D. Olender).

https://doi.org/10.1016/j.heliyon.2024.e37147
Received 17 June 2024; Received in revised form 27 August 2024; Accepted 28 August 2024
Available online 30 August 2024

1. Introduction

Antioxidants are key in the treatment of many complex diseases that are the result of oxidative stress and disturbed oxidative balance in the body. They are responsible for many protective effects and actions e.g. anti-inflammatory, anticancer and anti-ageing. Oxidative stress affects human metabolism and can lead to diseases such as diabetes, cardiovascular, metabolic syndrome, obesity and also neurodegenerative diseases by damaging neurons [1]. Current research on multifactorial diseases, including Alzheimer's (AD) and cancer, proves that designing new structures with therapeutic potential is essential to creating innovative structures that determine multi-target biological activity and use proven drugs with relatively low molecular weight. Among the antioxidant compounds of particular interest are antioxidants, especially polyphenols, which are crucial for the antioxidative defence mechanisms of cells and organisms [1].

AD concerns increasingly younger patients and is associated with an oxidative imbalance and a deficiency of reducing and antioxidant compounds. Moreover, the AD disease mechanism is correlated with the deficiency of the acetylcholine (ACh) neurotransmitter by cholinesterases. The greatest therapeutic hopes are associated with the use of acetylcholinesterase (AChE) inhibitors as well as glutamatergic antagonists of the N-methyl-D-aspartate receptor. The anticholinesterase inhibitors, although not preventing the progression of the AD disease, significantly improve the clinical symptoms of patients, especially in the cognitive sphere [2]. Moreover, different studies suggest that chronic inflammation is crucial to AD pathogenesis. For this reason, it is crucial to look for substances that suppress this process by inhibiting cyclooxygenase-2 (COX-2), the key compound of the eicosanoid biosynthetic pathway, which is the source of pro-inflammatory mediators [3]. COX-2 is produced during damage by inflammatory stimuli and is a key importance during inflammation, while cyclooxygenase-1 (COX-1) is present in nearly all tissues and primarily has 'housekeeping' functions [3]. Inflammation in neurons in the brain results in impaired acetylcholine conduction and, therefore, the possibility of developing dementia and AD. Acetylcholinesterase inhibitors, by reducing pro-inflammatory molecules and the expression of COX-1 and COX-2, reduce the inflammatory response and increase the level of Ach in the brain. Anti-inflammatory effects of acetylcholine cause that acetylcholine can inhibit the activity of COX-2, thereby reducing the production of prostaglandins and consequently resulting in inflammation. Moreover, it is suggested that COX-2 inhibitors cause greater acetylcholine potency and increase its availability in the brain [3]. For this reason, inflammation measured by COX-2 indicates the possibility of developing many diseases, including AD.

Developing effective treatment for AD is currently one of the major challenges for researchers. Diagnosing AD is an experience that radically changes the patient's life but also affects all members of his family. The limited ability to deliver drugs to the brain due to poor solubility, low bioavailability, and the impact of the blood-brain barrier (BBB) is a huge problem in the treatment of AD [4]. Therefore, it is essential to find effective treatments. Chalcones are pharmacologically significant molecules in this context. They constitute an innovative class of compounds with significant therapeutic potential in the fight against various diseases. Their structure is an excellent scaffold for developing new drugs [5]. Moreover, these structures can enter easily into different active sites and, therefore, have an affinity with other enzymes and receptors. Chalcone derivatives have a broad spectrum of therapeutic effects, including antioxidant, anti-inflammatory, anti-neurodegenerative, anticancer, antiviral, and antiprotozoal (Fig. 1) [6–9]. Significantly, it has been proven that different strategies for the synthesis of chalcones and also their structural modifications are effective in developing new drugs, differing in potency and mechanism of action due to interactions with various target proteins [10].

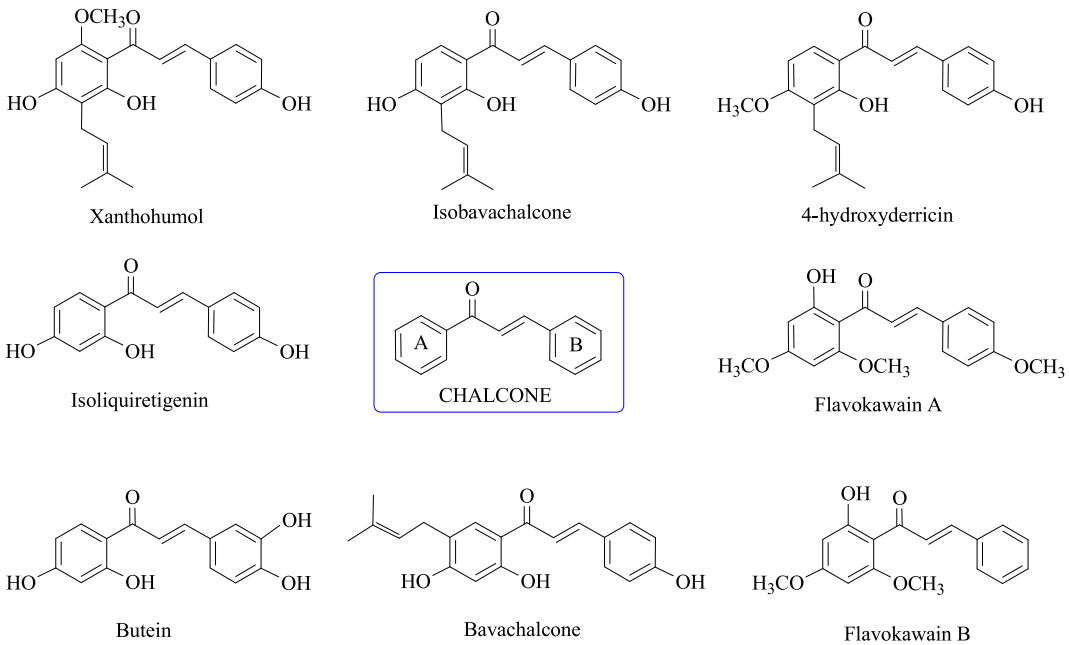

Fig. 1. Naturally-occurring chalcone and its derivatives with biological activity.

It was found that the introduction of electron-donating groups (EDG) into the molecule induces an enhanced AChE inhibitory activity, while electron-withdrawing groups (EWG) result in this activity [11]. Analogs without substituents in aromatic rings showed weaker activity than the ortho-substituted derivatives with a hydroxy group (OH) at ring A. Additionally, it was observed that the presence of chlorine at ring A resulted in reduced activity. Also, the number of introduced methoxy groups (OCH_3) caused differences in the AChE inhibition. Disubstituted analogs were characterized by higher activities than monosubstituted ones. Among the numerous substitutions on B rings, ortho substitution was the most promising position for BChE inhibition, while the meta and para substitutions on the B ring reduced the activity. Further, introducing OCH_3 in the meta and para positions also positively affected the BChE inhibitory potential [12]. Curcuminoid chalcones have promising biological potential as compounds that bear structural elements characteristic of curcumin and chalcone skeletons [13,14]. The chalcones with OH and OCH_3 groups in ring B reduced the expression of antioxidant enzymes that could degrade reactive oxygen species (ROS), which is good news in multifactor diseases. The results also showed that derivatives containing OH and OCH_3 groups in rings A and B or in only rings B showed significant toxicity towards the Caco-2 cell line [13]. Furthermore, according to molecular hybridization, combining the chalcone structure with other biologically active units is advantageous. Our earlier biological studies also showed that curcuminoid chalcone-ibuprofen hybrids showed antioxidant activity. The same hybrids also inhibited AChE and BChE and were more active than their substrates.

Among chalcones, our attention primarily focused on *bis*-chalcones, compounds containing two chalcone moieties in one molecule (Fig. 2). In this type of structure, the twin α,β-unsaturated ketone moieties can be separated by a central unit derived from diformylarene or diacetylarene. In classical *bis*-chalcones, a central aromatic ring is usually substituted at C-1, C-3, or C-1, C-4. Moreover, aryl rings derived from benzaldehyde or acetophenone contain different atoms and groups like F, Cl, OCH_3, or OH or are condensed with heterocyclic rings directly or *via* a linker [15].

Bis-chalcone-type compounds are an exceptional chemical scaffold with multifarious biological activities. Due to their valuable properties, they are extremely attractive and intensively studied structures with a broad spectrum of possible biological activities. Many *bis*-chalcone derivatives have already been tested as antimicrobial, anticonvulsant, antidiabetic, antioxidant, antitubercular, anti-HIV, antiamoebic and above anti-inflammatory agents, as well as inhibitors for carbonic anhydrases and AChE [15]. Some showed antimalarial [16] and antiproliferative activity [17,18]. *Bis*-chalcones also inhibited *in vitro* aggregation and promoted the disintegration of α-synuclein - a protein whose deposition is considered one of the causes of Parkinson's disease (PD) [19] and acted as inhibitors of α-glucosidase [20]. Literature reports indicate that these chalcone derivatives showed anticancer properties [21–23]. *Bis*-chalcones containing methoxy group or fluorine atom exhibit more potent cytotoxicity than curcumin and other *bis*-chalcone analogs tested [24]. Another study showed that the *bis*-chalcones consisting of substituted 4-hydroxy chalcones structures with an ether moiety in a three-carbon unsaturated ketone linker resulted in higher inhibition than the standard 4-hydroxy chalcone series. The importance of *bis*-analogs for AChE inhibition was also observed [25].

In light of the presented properties, compounds based on the structure of *bis*-chalcone show great potential in medicinal chemistry because they seem to be good candidates for new drugs in the treatment of neurodegenerative diseases and may constitute a potential weapon in new therapeutic strategies. On the other hand, the described in the literature studies of *bis*-chalcones seem to be insufficient still, so inspired by the latest literature reports, we decided to synthesize several compounds having the chemical structure of *bis*-chalcone **(3a-3d)** in which α,β-unsaturated ketone moiety is available to evaluate their potency in neurodegenerative diseases and cytotoxicity towards neuronal cell line (HT-22) with the expectation to find out new candidate molecules which may direct further our scientific works.

2. Results and discussion

2.1. Synthesis and characterization of bis-chalcone derivatives

The synthesis of *bis*-chalcone derivatives was performed as described in the Materials and methods section. These derivatives were synthesized in one-pot reactions using readily available starting materials, i.e., aromatic methylketones and dialdehyde. Terephthalaldehyde **(1)** was the aldehyde starting material for performing our syntheses. Aromatic dialdehyde **(1)** reacted with appropriate carbanion formed in an alkaline medium from aromatic ketone including acetophenone **(2a)**, 4-hydroxy-3-methoxyacetophenone (apocynin) **(2b)**, 2-hydroxy-4-methoxyacetophenone (paeonol) **(2c)** and 4-hydroxyacetophenone (piceol) **(2d)**. In these reactions, β-hydroxy carbonyls were formed as intermediates. Next, under-acidified, appropriate *bis*-chalcone was produced. The selected acetophenones and terephthalaldehyde formed the corresponding *bis*-chalcones in the Claisen-Schmidt reaction using our procedure known from the literature data used for curcuminoid chalcones with modifications [13]. Terephthalaldehyde was reacted with twice

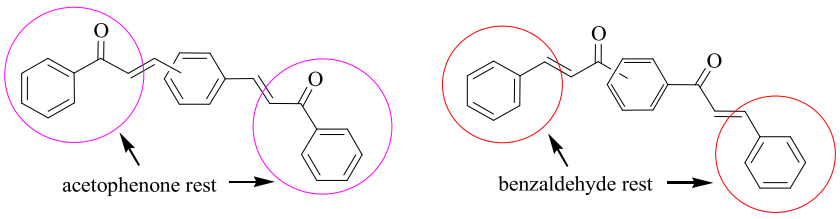

Fig. 2. The compounds *bis*-chalcone type.

the excess of unsubstituted or substituted methylketones to yield the *bis*-chalcones expected in all products obtained. The suitable substrates were dissolved in ethanol. To the solution of the appropriate methylketone, sodium hydroxide (NaOH) as the aqueous solution was added. Then, an ethanolic solution of terephthalaldehyde was added at room temperature. These reactions run with final good yields (79–88 %). Analyzing the yield of condensation reactions, it was noticed that the highest yield was recorded in the case of obtaining *bis*-chalcone **3a**, without substituents (88 %). *Bis*-chalcone **3d**, containing hydroxy groups in its structure, was obtained with a slightly lower yield. The lowest yield was observed for derivatives containing hydroxy and methoxy groups (**3b** and **3c**).

As a result, four *bis*-chalcones **(3a–3d)** were obtained without or with OH and OCH_3 groups (Scheme 1).

In the case of the reaction of **1** with **2b, 2c** or **2d**, in addition to the main products **3b, 3c** and **3d**, by-products were also present in the reaction mixture, as shown by the TLC chromatography. After the column chromatography separation with an appropriately selected mobile phase, two compounds with different R_f values were obtained. By-products **3bb**, **3cc** and **3dd** were created with a yield not exceeding 15 %. In the case of the reaction of terephthalaldehyde with benzaldehyde, by-product formation was not observed. The observed relation is likely due to the bearing of electron-donating substituents in aromatic ketones, which facilitated the reaction.

The structures of the purified *bis*-chalcones and by-products were confirmed with the spectral data (EI-MS, FT-IR, ^{1}H NMR and ^{13}C NMR). Mass spectrometry analysis using the EI-MS method confirmed the synthesis of four *bis*-chalcones **(3a-3d)** (Fig. 3). In the EI-MS spectra of products synthesized, the compound's molecular mass was supported by the molecular ions corresponding to the values consistent with the calculated molecular weights of the derivatives. In the case of the reaction of **1** with **2b, 2c** or **2d.** After analyzing mass spectra of by-products, monocondensation products **(3bb-3dd)** were confirmed (Fig. 3).

In the IR spectra of the derivatives obtained with the *bis*-chalcone structure, a band characteristic of the stretching vibrations in the carbonyl occurring in the alkyl chain connecting the rings was found. The substituents that occurred in the aromatic system influenced the position of the C=O or C=C signals. The band characterized for the C=O group occurred at 1653 cm^{-1} for the compound without substituents (**3a**). In the case of compound **3d** bearing hydroxyl in the C-4 position of the aromatic ring, the C=O band at 1637 cm^{-1} was observed. Moreover, the occurrence of OCH_3 besides OH in the phenyl rings also influenced the wavenumber of the C=C band in compounds **3b** and **3c** (1565 and 1564 cm^{-1}) compared to compounds **3a** and **3d** (1604 and 1602 cm^{-1}). The methoxyl as an electron donating group impairs the C=C bond. The broad bands for stretching vibrations O-H bonds of phenol groups were present at about 2900 cm^{-1} in the spectra of **3b-3d**. Moreover, in the spectra of these compounds, there is a band of deformation vibrations of C-H bonds, characteristic of trans-alkenes, and a band of stretching vibrations of the same bonds. The spectra of compounds **3a-3d** also include bands associated with the presence of the aromatic ring (Fig. 3).

The interpretation details of NMR spectra (proton and carbon-13) confirming that the main products are compounds with a *bis*-chalcone structure (Fig. 3). The ^{1}H NMR spectra showed that all protons in the unsaturated propenone chain appeared as two doublets appropriately between 8.19 and 7.91 ppm (Hβ) and 7.88–7.69 ppm (Hα). For example, in the spectrum obtained for compound **3a**, protons belonging to this group appeared in the form of doublets at 8.07 and 7.80 ppm. High values of the *J* coupling constants (*J* approximately 15 Hz) indicate that the obtained compounds exist as trans isomers. ^{1}H NMR spectra of compounds **3b** and **3c** with chemical shifts next to 3.90 ppm certify the presence of the methoxy groups. For example, in derivative **3b**, singlets belonging to the six protons of the methoxy groups were present at the 3.83 ppm position. For the derivatives **3b-3d**, the hydroxyl protons in the phenol moiety were visible as singlets (at 10.03 ppm for **3b**). Moreover, the signals at about 7.00–8.32 ppm, mainly as doublets, correspond to the aromatic protons. In the ^{13}C NMR spectra, the structure of the obtained derivatives was certified by the signal coming from two carbonyl groups present in the aliphatic chain (189 ppm for **3a**), signals belonging to the Cα and Cβ carbons in the vinyl moiety, as well as signals coming from the OCH_3 groups present in derivatives **3b** and **3c**. The formation of a hydrogen bond between the hydroxyl at the C-2 position of the aromatic ring and oxygen in the carbonyl group for compound **3c** caused a shift in the carbon resonance of C=O downfield to 192.63 ppm for compound **3c** in the comparison with compound **3a**. The IR spectra analysis showed that the carbonyl stretching vibrations appeared between 1653 and 1636 cm^{-1}. The C=O stretching has a strong absorption band, usually above the 1650 cm^{-1} region. The bands of the C=O group in the *bis*-chalcones spectra were observed at a lower wavenumber than a typical carbonyl band due to conjugation with the olefinic carbon-carbon bond.

All the spectral results were presented in the Materials and methods section. The spectra (EI-MS, FT-IR, ^{1}H and ^{13}C NMR) were added in the Supplementary Materials (Figs. B.1-19). Moreover, spectrophotometric characteristics were performed for compounds obtained **(3a-3d)**. The presence of OCH_3 groups in the *bis*-chalcones leads to the shift toward a higher wavelength (bathochromic effect). The electron delocalization in the *bis*-chalcones is stabilized by methoxyl because it is an electron-donating group. Isomeric compounds, i.e. **3b** and **3c**, have similar UV–Vis spectra, which is caused by a slight dependence of radiation absorption in this band of

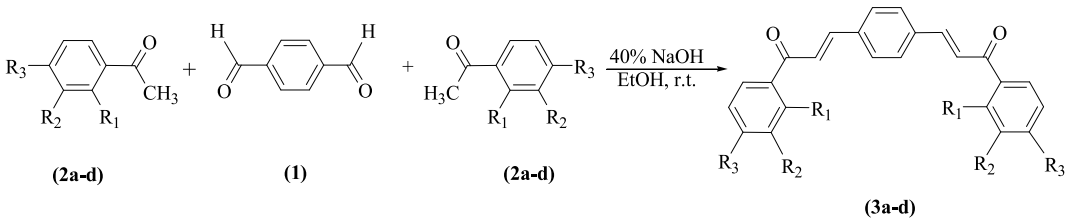

(2a-d) (1) (2a-d) (3a-d)

2a, **3a**: R_1=H, R_2=H, R_3=H; **2b**, **3b**: R_1=H, R_2=OCH_3, R_3=OH; **2c**, **3c**: R_1=OH, R_2=H, R_3=OCH_3; **2d**, **3d**: R_1=H, R_2=H, R_3=OH

Scheme 1. *Bis*-chalcones (3a-d) synthesis path.

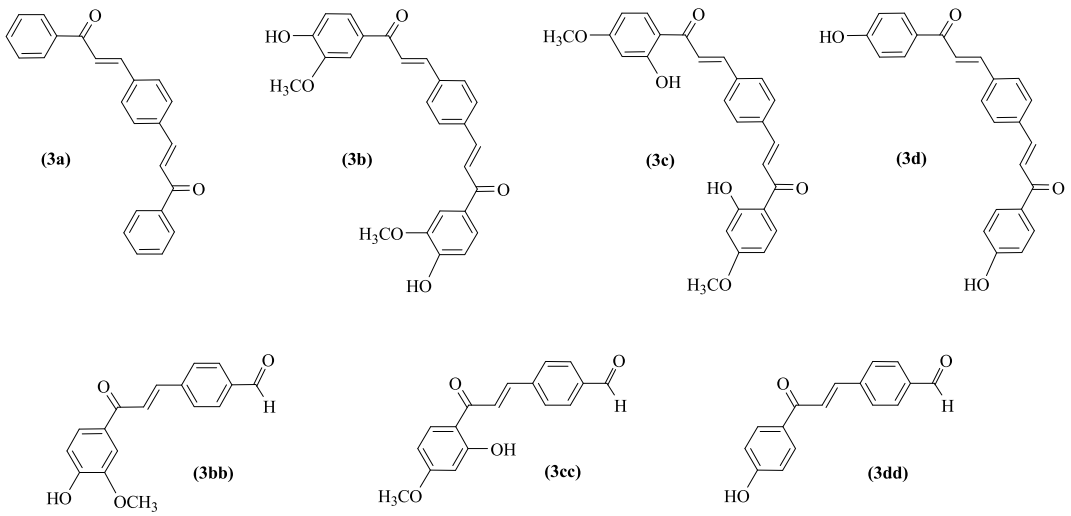

Fig. 3. The structures compounds obtained.

electromagnetic radiation on the arrangement of functional groups within the molecule of the compound tested (Fig. 3).

2.2. Biological studies

The *bis*-chalcones synthesized were examined in a biological study for their potency as anti-neurodegenerative agents.

2.2.1. Antioxidant activity

2.2.1.1. Hydroxyl radical antioxidant capacity (HORAC). In this work, we evaluated the high capacity of all four tested compounds to block the fluorescent probe's radical hydroxyl oxidation (Table 1).

2.2.1.2. Effect on the activity of antioxidant enzymes. We checked the influence of *bis*-chalcones tested on glutathione reductase (GR) and glutathione peroxidase (GPx) activities (Table 2). Besides, the effect of *bis*-chalcones on catalase (CAT) activity was evaluated (Table 2).

The compound **3b** decreased the activity of all three enzymes GR, GPx, and CAT (by 4.5 ± 2.0, 16.2 ± 2.0 and 90.2 ± 3.6 %, respectively). The compound **3c** reduced GR and GPx activities by 23.4 ± 2.3 % and 27.2 ± 3.6 %, respectively, while the **3d** decreased GPx activity only (by 22.0 ± 3.2 %) and the **3a** had a negative effect on GR and CAT (reduction of activities by 34.0 ± 3.1 % and 30.2 ± 4.5 %, respectively).

2.2.2. Anti-inflammatory activity

Inhibition of the COX-2 enzyme by *bis*-chalcones is shown in Table 3.

The results obtained from our study indicate that three tested compounds appeared to have the ability to inhibit COX-2 with the most active **3c**. By analyzing the *in vitro* results, it was found that *bis*-chalcone derivatives had higher selectivity towards COX-2 than the mono derivatives [14]. The experimental data suggest that the *bis*-chalcones tested can reduce the inflammatory response induced by COX-2, which can be helpful in the context of the degeneration of the nervous system problem.

2.2.3. Anticholinergic activity

In this work, the modified Elman's method was used to investigate the anti-AChE and anti-BChE effect of the four *bis*-chalcones tested. Rivastigmine and magniflorine, well-known AChE and BChE inhibitors were used as positive controls.

Table 1
Effect of *bis*-chalcones on HORAC activity.

Compound	Gallic acid equivalents (μg/mL)
3a	71.6 ± 1.9
3b	48.2 ± 2.2
3c	60.9 ± 2.1
3d	73.0 ± 3.7

The mean values ± SEM from three measurements are presented (n = 3).

Table 2
Effect of *bis*-chalcones on GPx, GR and CAT activity.

Compound	GPx		GR		CAT	
	Inhibition (%)	Inhibition (nmol depleted NADPH/min)	Inhibition (%)	Inhibition (nmol depleted NADPH/min)	Inhibition (%)	Inhibition of the H_2O_2 depletion ($mm/dm^3/min$)
3a	–	–	34.0 ± 3.1	1276 ± 116	30.2 ± 4.5	0.12 ± 0.01
3b	16.2 ± 2.0	32.2 ± 4.0	4.5 ± 2.0	168 ± 75	90.2 ± 3.6	0.29 ± 0.01
3c	27.2 ± 3.6	54.1 ± 7.2	23.4 ± 2.3	881 ± 86	–	–
3d	22.0 ± 3.2	43.8 ± 5.0	–	–	–	–

"-" - not active. The mean values ± SEM from three measurements are presented (n = 3).

Table 3
Inhibition of COX-2 enzyme by *bis*-chalcones.

Compound	COX-2 Inhibition (%)	Equivalent Concentration of Acetylsalicylic Acid (mg/mL)
3a	–	–
3b	13.5 ± 0.2	6.9 ± 0.1
3c	29.4 ± 0.3	8.8 ± 0.1
3d	3.4 ± 0.1	5.6 ± 0.1

"-" - not active. The mean values ± SEM from three measurements are presented (n = 3).

The results obtained exhibited that the compounds tested showed excellent activity (Table 4). The enzymes were inhibited by all compounds tested. All *bis*-chalcones were more efficient against BChE than AChE except the **3b,** which showed adverse effect. The compound **3a** demonstrated the greatest inhibition of BChE. The greatest inhibition of AChE was shown by compound **3b** with electron-donating groups (OCH_3) in the aromatic ring of the *bis*-chalcone. The literature [26] showed that some *bis*-chalcone derivatives presented notable values in the μM concentration, where the compound with moiety phenyl showed the best inhibition. However, when electron-donating groups were present in the aromatic system of *bis*-chalcones, the activity of them was decreased.

2.2.4. The mouse hippocampal neuronal cell line (HT-22) study

2.2.4.1. Resazurin reduction assay. Conducted experiments revealed that after 24 h of exposure of HT-22 cells to the **3d**, this compound decreased resazurin levels (by 29.39 %, compared to the control), but only at the concentration of 10 μM (Fig. 4A). The compound **3c** reduced resazurin concentrations at 50 and 100 μM (73.27 and 80.17 %, respectively, compared to untreated ones) (Fig. 4B). After the same cultivation time, the **3b** also decreased resazurin levels at 50 and 100 μM (42.06 and 84.66 %, respectively, compared to the control) (Fig. 4C). In cells exposed to the **3a**, 100 μM of the studied compound increased in resazurin concentration by 13.42 % compared to DMSO-treated cells (Fig. 4D).

Obtained data shows that compounds **3b** and **3c** strongly decreased cell metabolism, which can be an effect of toxicity and/or decreased cell proliferation. Conversely, compound **3a** increased in the cell metabolism or the number of cells. Interestingly, compound **3d** decreased cell metabolism only at 10 μM concentration (Fig. 4). In the authors' opinion, 10 μM compound **3d** could decrease cell number while higher concentrations (50 and 100 μM) increase the activation of detoxification enzymes, increasing cell metabolism. Therefore, experiments showed that paradoxical 50 and 100 μM of **3d** did not affect resazurin reduction. Similar results were observed in the Jurkat cell line in which 10 nM vincristine decreased cell metabolism measured by resazurin test while 1 μM vincristine increased resazurin reduction compared to 10 nM concentration [27]. In the mentioned paper, authors suggest that the mentioned phenomenon is probably an effect of activation and increase in cytochrome P450 family 3A.

2.2.4.2. LDH release. After 24 h of the exposure of HT-22 cells to increasing concentrations of the **3d**, it can be seen that this compound increased the release of lactate dehydrogenase (LDH) (by 14.49 %, compared to the untreated cells) but only at the concentration of 100 μM (Fig. 5A). Also, the increase in the release of LDH occurred in the case of the **3b** applied at the most concentration of

Table 4
Inhibition of AChE and BChE by *bis*-chalcones.

Compound	AChE %	AChE (μg/mL) (equivalent concentration of reference compound)		BChE %	BChE (μg/mL) (equivalent concentration of reference compound	
		Rivastigmine	Magniflorine		Rivastigmine	Magniflorine
3a	35.7 ± 2.0	0.21 ± 0.01	0.14 ± 0.01	85.2 ± 1.9	0.25 ± 0.01	0.33 ± 0.01
3b	75.9 ± 11.2	0.40 ± 0.06	0.27 ± 0.04	69.2 ± 4.6	0.20 ± 0.01	0.27 ± 0.02
3c	59.9 ± 4.8	0.37 ± 0.03	0.24 ± 0.02	71.0 ± 5.7	0.21 ± 0.02	0.28 ± 0.02
3d	47.3 ± 1.8	0.28 ± 0.01	0.19 ± 0.01	82.7 ± 4.8	0.24 ± 0.01	0.32 ± 0.02

The mean values ± SEM from three measurements are presented (n = 3).

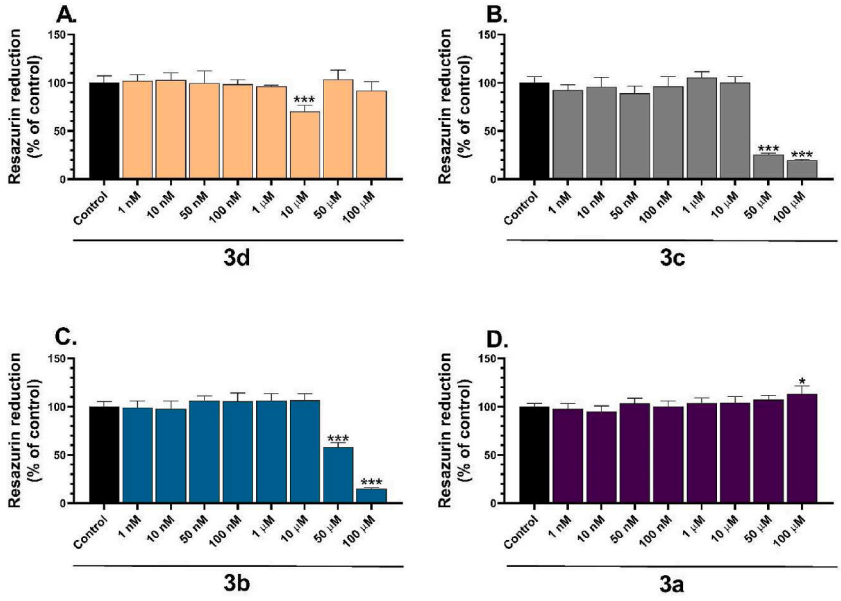

Fig. 4. Effect of increasing concentrations of tested: **3a** (D), **3b** (C), **3c** (B), and **3d** (A) compounds on the level of resazurin reduction after 24 h exposure of HT-22 cells. Data are expressed as mean ± SD of three independent experiments. *$p < 0.05$, **$p < 0.01$, and ***$p < 0.001$ *vs.* the control cells.

100 μM (34.56 %, compared to the control) (Fig. 5C). On the other hand, in the case of the **3c**, both compounds decreased the release of LDH (by 24.49 and 29.37 %, respectively, compared to the untreated ones), but only at the concentrations of 50 and 100 μM (Fig. 5B). In the present study, compound **3a** was inactive in the LDH release in HT-22 cells (Fig. 5D). Increased LDH release caused by compounds **3d** and **3b** confirmed the toxicity of these compounds at 100 μM and suggests cell damage. In the case of the **3c,** a substantial decrease in LDH release resulted from the strong toxicity which was indicated by a decreased resazurin reduction test. High toxicity causes a rapid release of LDH levels and its degradation by proteolytic enzymes released from decayed cells [28]. Therefore, a decrease in LDH was observed in our work.

2.2.4.3. Protein expression analysis. Protein expression analysis in HT-22 was compared for compounds obtained and the control.

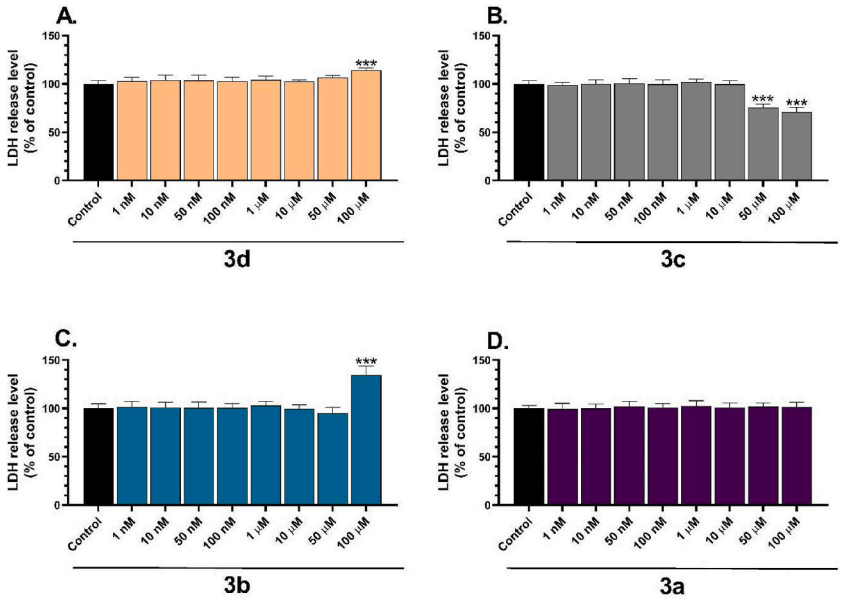

Fig. 5. Effect of increasing concentrations of the compounds tested: **3a** (D), **3b** (C), **3c** (B), and **3d** (A) on LDH release after 24 h exposure of the HT-22 cells. Data are expressed as mean ± SD of three independent experiments. *$p < 0.05$, **$p < 0.01$, and ***$p < 0.001$ *vs* the control cells.

Experiments conducted for 24 h revealed that compounds **3a**, **3c,** and **3d** at the concentration of 10 μM decreased PGC-1α protein expression by 17.72, 33.82 and 35.87 %, respectively (Fig. 6A). However, compound **3b** at 10 μM increased PGC-1α protein expression by 26 %. Similarly, compared to the control, compounds **3c** and **3d** decreased PPARγ protein expression by 23.73 and 13.41 %, respectively (Fig. 6B). The compound **3a** didn't affect PPARγ protein expression, while compound **3b** increased PPARγ protein expression by 194.52 % (Fig. 6B). The compounds **3a**, **3c**, and **3d** increased IκBα expression in HT-22 cells by 21.24, 20.22, and 16.72 %, respectively, at 10 μM (Fig. 6C). However, compound **3b** didn't affect IκBα protein expression in HT-22 cells. In the case of the phosphorylated form of IκBα, compounds **3a, 3b, 3c**, and **3d** increased p(S32)-IκBα levels by 231.14 %, 412.15 %, 71.02 %, and 142.00 %, respectively (Fig. 6D).

Protein analysis revealed that after 24 h of exposure to compounds **3d** and **3a**, an increase in ARNT protein expression in HT-22 cells (12.20 and 30.47 %, respectively) (Fig. 7A). On the other hand, compound **3b** decreased ARNT protein expression by 47.77 %. At the same time, compound **3c** didn't change ARNT levels in HT-22 cells (Fig. 7A). In the case of AhR, the mentioned compound, similarly to ARNT, changes protein expression. Indeed, compounds **3d** and **3a** increased ARNT protein expression in HT-22 cells by 14.58 and 43.62 %, respectively (Fig. 7C). On the other hand, compound **3b** decreased ARNT protein expression by 64.59 %, while compound **3c** didn't change ARNT levels in HT-22 cells (Fig. 7C). All studied compounds increased superoxide dismutase-1 (SOD1) protein expression by 23.37, 41.25, 46.55, and 24.67 %, respectively (Fig. 7B). However, only compounds **3a**, **3c** and **3d** increased NF-κB protein expression by 16.22, 31.08 and 23.34 %, respectively (Fig. 7D). The compound **3b** didn't change NF-κB protein expression in HT-22 cells.

To date, it is well-described that aryl hydrocarbon receptor (AhR) and AhR nuclear translocator (ARNT) regulate other inflammation, neurotoxicity, and immune cell recruitment in various neurodegenerative diseases [29]. Moreover, it has been described that AhR agonists can inhibit nuclear factor kappa B (NF-κB)-mediated, which is a crucial inflammatory signalling mediator [30]. However, the NF-κB-based transduction of the pro-inflammatory signal to nuclei requires the phosphorylation of IκBα, followed by its proteasome-related degradation. The cross-talk between AhR and peroxisome proliferator-activated receptor gamma (PPARγ) has also been described [31]. Our data shows that compound **3b** decreases AhR and ARNT protein expression (Fig. 7A–C). Moreover, compound **3b** strongly increases PPARγ protein expression and PPARγ coactivator (PGC-1α) (Fig. 6B–A). Interestingly, despite the lack of changes in the NF-κB and IκBα protein expression level, the amount of phosphorylated (p(S32)) IκBα protein expression increased (Fig. 6D). Therefore, we cannot exclude the pro-inflammatory properties of this compound. Our data shows that compounds **3d**, **3c** and **3a** increase AhR Fig. 7C) and ARNT protein level expression (Fig. 7A) while decreasing PPARγ and its coactivator PGC-1α (Fig. 6B–A). Moreover, the mentioned compounds increase in NF-κB (Fig. 7D) and IκBα levels (Fig. 6C). Therefore, we believe that compounds **3d**, **3c** and **3a** do not initiate the inflammation process. To date, SOD-1 expression can be controlled by PPARγ [32] and AhR [33]. Therefore, our data in which all studied compounds increase SOD1 protein expression are consistent with current knowledge about PPARγ and AhR molecular pathways.

Collectively, our data concerning AhR, ARNT, PGC-1α, PPARγ, p(S32)-IκBα, IκBα and NF-κB suggest that compounds **3d**, **3c**, and **3a** act through the AhR pathway, while the compound **3b** works mainly through the PPARγ molecular pathway.

2.3. Computational studies

In our study, we focused our attention on the *in silico* analysis of the highest occupied molecular orbitals (HOMO) and lowest occupied molecular orbitals (LUMO) as important factors for the description of compounds' properties from the standpoint of their electrical and optical nature. In our paper, we used the TD-DFT method to investigate the spectra of analytes **3a–3d**. Their geometry

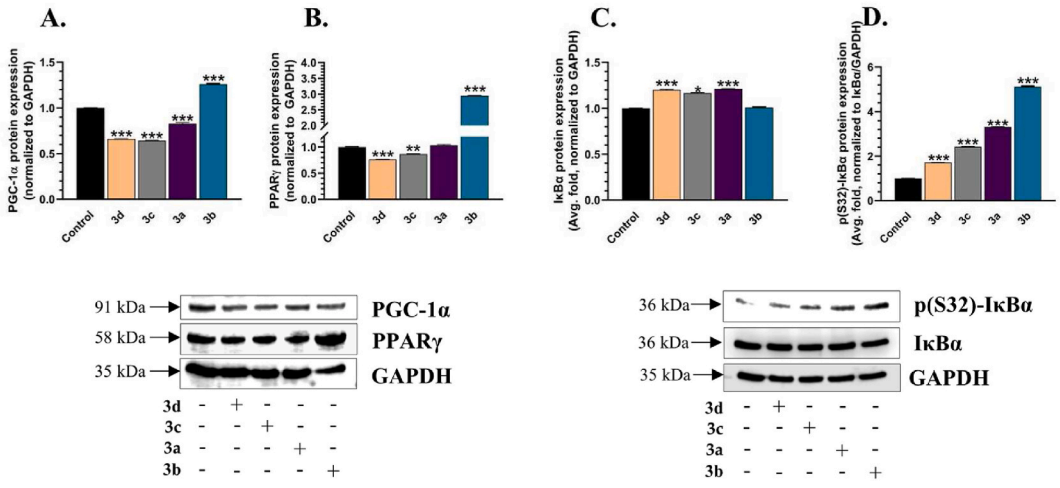

Fig. 6. PGC-1α (A), PPARγ (B), IκBα (C), p(S32)-IκBα (D), and GAPDH protein expression of compounds tested after 24 h of exposure **3d** and **3a** in HT-22 cells. Data are expressed as mean ± SD of three independent experiments. *p < 0.05, **p < 0.01, and ***p < 0.001 *vs* the control cells.

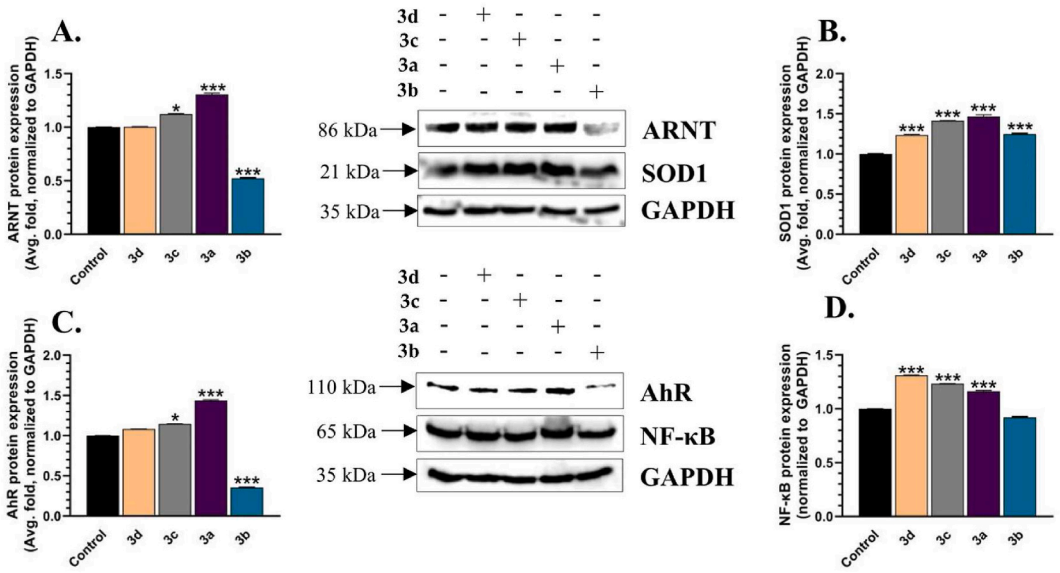

Fig. 7. ARNT (A), SOD1 (B), AhR (C), NF-κB (D), and GAPDH protein expression of compounds tested after 24 h of exposure compounds **3d** and **3a** in HT-22 cells. Data are expressed as mean ± SD of three independent experiments. *p < 0.05, **p < 0.01, and ***p < 0.001 *vs* the control cells.

was previously optimized (B3LYP/6-31G(d,p) or PBE1PBE/6-31G(d,p) approaches *in vacuo* or in the presence of solvents: chloroform, methanol, and water). The vertical excited states were calculated for each optimized rotamer of compounds **3a–3d** at the B3LYP/6–311++G(2d,3p) or PBE1PBE/6–311++G(2d,3p) levels of theory in the gas phase, as well as in chloroform, methanol, and water (IEFPCM). On this account, using water as the solvent for the simulation of the cell environment for compounds **3a–3d**, we estimated several descriptors (Table 5), i.e., electronegativity (χ), chemical hardness (η) and electronic potential, first ionization potential (I), and electron affinity (A) using Koopman's theorem [34]. For derivative **3b,** we noticed the lowest value of the chemical hardness (η). On the contrary, the highest value of the η parameter corresponded to *bis*-chalcone **3a**. As far as chemical potential is concerned, ligand **3a** has the most negative chemical potential value. The most electronegative molecule was molecule **3a**, too. Notably, similar HOMO-LUMO gap values and related descriptors were reported for other chalcone derivatives [35–38].

The LUMO (B) and HOMO (A) orbitals of compounds **3a**–**3d** are given in Figs. 8–11 (A,B), respectively (TD-DFT methodology), and they were observed. Mainly overall aromatic moieties, especially covering central phenyl moiety with substituted -C=C- linkers.

Theoretical UV–Vis spectra of compounds **3a**–**3d** considering the reaction field of chloroform or methanol are given in the Supplementary Materials (Fig. D.3) and are computed using B3LYP or PBE0 functional, respectively. We analyzed vertical excited states and the estimated maxima of absorption λ_{max} (Table 6). It turned out that the first excited state of the analytes corresponded to their maximum absorption. Using the B3LYP or PBE1PBE functionals, we obtained the lowest λ_{max} values for derivative **3a**. The *bis*-chalcone **3b** was characterized by the significantly highest λ_{max} values. The first excited state (λ_{max}) for compound **3a** relates mainly to the 407.85 (chloroform, B3LYP functional), 408.29 (methanol, B3LYP functional), 391.71 (chloroform, PBE0 functional) or 391.63 nm (methanol, PBE0 functional) and an electron excitation from orbital 89 to orbital 90 as a HOMO → LUMO transition. We also noticed that the HOMO−LUMO contribution relative to the first excited state, calculated as duplicated coefficient square, is 96 % (chloroform, B3LYP functional), 97 % (methanol, B3LYP functional), 94 % (chloroform, PBE0 functional) or 96 % (methanol, PBE0 functional).

The UV spectrum and the 1st excited state (λ_{max}) of compound **3b** are described by the following parameters: electron excitation from orbital 113 to orbital 114 as a HOMO → LUMO at the 432.06 (chloroform, B3LYP), 434.79 (methanol, B3LYP), 410.47

Table 5
Computed global reactivity parameters [eV]: **E_{HOMO}** – energy of the HOMO orbital, **E_{LUMO}** – energy of the LUMO orbital, **HOMO-LUMO gap** – absolute value of the HOMO–LUMO gap, water as solvent.

Compound	E_{HOMO}	E_{LUMO}	HOMO-LUMO gap	I	μ	A	χ	η
B3LYP								
3a	−6.5079	−3.1380	3.3699	6.5079	−4.8230	3.1380	4.8230	1.6849
3b	−6.2766	−3.0412	3.2355	6.2766	−4.6589	3.0412	4.6589	1.6177
3c	−6.2954	−2.9731	3.3223	6.2954	−4.6343	2.9731	4.6343	1.6611
3d	−6.4021	−3.0376	3.3644	6.4021	−4.7199	3.0376	4.7199	1.6822
PBE1PBE								
3a	−6.7292	−3.0052	3.7239	6.7292	−4.8672	3.0052	4.8672	1.8620
3b	−6.4766	−2.9067	3.5699	6.4766	−4.6917	2.9067	4.6917	1.7849
3c	−6.5068	−2.8379	3.6689	6.5068	−4.6724	2.8379	4.6724	1.8345
3d	−6.6168	−2.9029	3.7138	6.6168	−4.7599	2.9029	4.7599	1.8569

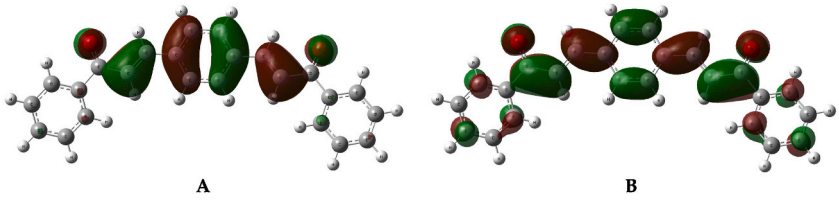

Fig. 8. Orbitals HOMO (A) and LUMO (B) of **3a**.

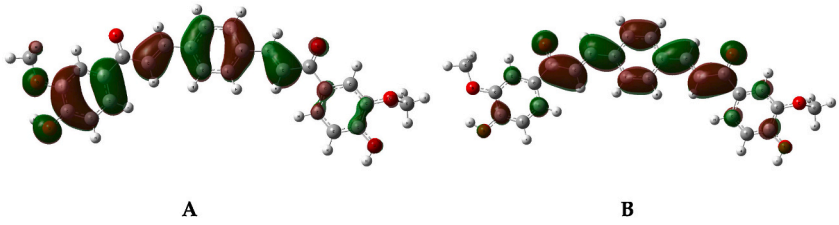

Fig. 9. Orbitals HOMO (A) and LUMO (B) of **3b**.

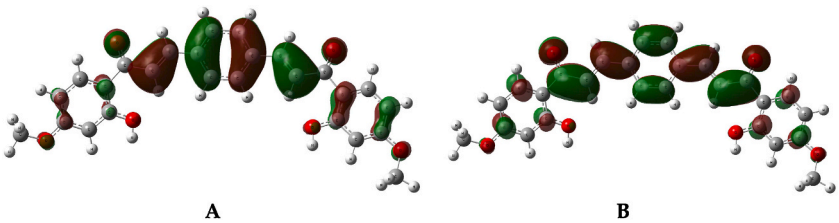

Fig. 10. Orbitals HOMO (A) and LUMO (B) of **3c**.

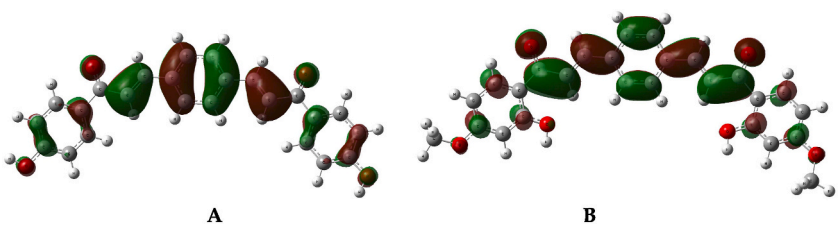

Fig. 11. Orbitals HOMO (A) and LUMO (B) of **3d**.

(chloroform, PBE0) or 412.68 nm (methanol, PBE0). Their first excited state is 97 % (chloroform, B3LYP), 98 % (methanol, B3LYP), 94 % (chloroform, PBE0) or 94 % (methanol, PBE0). Moreover, in the reaction field of methanol in general, we observed a slight change of the spectral band position to a longer wavelength in the theoretical UV spectra of chalcones. The analysis of calculated UV–Vis spectra showed good accordance with the experimental spectrum (especially with the use of PBE1PBE functional).

In the next step, we focused our attention on the interactions of *bis*-chalcones **3a**–**3d** with selected biological targets. We used the COX-2 active site complexed with celecoxib (3ln1.pdb) [39,40] considering the proposed mechanism of chalcones' action as anti-inflammatory agents. Nine poses with the lowest negative value of binding affinity were obtained for each ligand **3a**–**3d.** Analyzing the optimized ligands [41] docked to the protein 3ln1.pdb [42], we concluded that the estimated during the docking protocol binding affinity was as follows: 7.900, −9.500, −9.800, and −8.900 kcal mol^{-1} for derivatives **3a**–**3d**, respectively (Fig. 12). The resultes from absolute values of the binding affinity were significantly higher in comparison with the value (−7.300 kcal mol^{-1}) computed for the docked **H0** analog (its structure is given in Fig. D.1 in the Supplementary Materials). From this standpoint, we noticed that the most active seemed to be analogue **3c,** as it is complex within the 3ln1.pdb protein was stabilized by three hydrogen bonds formed by Asn19, Cys26 and Gly30 (Figs. D.2-D.3 in the Supplementary Materials). It also turned out that the inactive with the COX-2 derivative **3a** was located differently among other ligands. Several hydrogen contacts were formed by **3c** within the cavity, namely (Fig. D.3 in the Supplementary Materials): with Asn19: N-H…H-O ($d = 2.933$ Å, $\theta = 97.04°$), and N-H…O=C ($d = 3.275$ Å, $\theta = 58.61°$) or with Cys26: O-H…O=C ($d = 2.729$ Å, $\theta = 80.12°$) or with Gly30: O-H…O=C ($d = 2.009$ Å, $\theta = 127.15°$), and O-H…N ($d =$ Å, $\theta =$

Table 6
The 1st excited states of compounds **3a–3d** related to the λ_{max} compounds in chloroform or methanol.

Compound	Environment	Energy [eV]	λ [nm]	f	Orbital transition
B3LYP					
3a	chloroform	3.0399	407.85	1.5612	89 → 90
	methanol	3.0367	408.29	1.5777	
3b	chloroform	2.8696	432.06	1.3160	113 → 114
	methanol	2.8516	434.79	1.2849	
3c	chloroform	2.9232	424.14	1.5003	
	methanol	2.8997	427.58	1.3973	
3d	chloroform	2.9930	414.25	1.6759	97 → 98
	methanol	2.9802	416.02	1.6523	
PBE1PBE					
3a	chloroform	3.1652	391.71	1.5536	89 → 90
	methanol	3.1659	391.63	1.5915	
3b	chloroform	3.0206	410.47	1.4876	113 → 114
	methanol	3.0044	412.68	1.4507	
3c	chloroform	3.0633	404.74	1.6324	
	methanol	3.0453	407.13	1.5385	
3d	chloroform	3.1287	396.28	1.7567	97 → 98
	methanol	3.1182	397.62	1.7373	

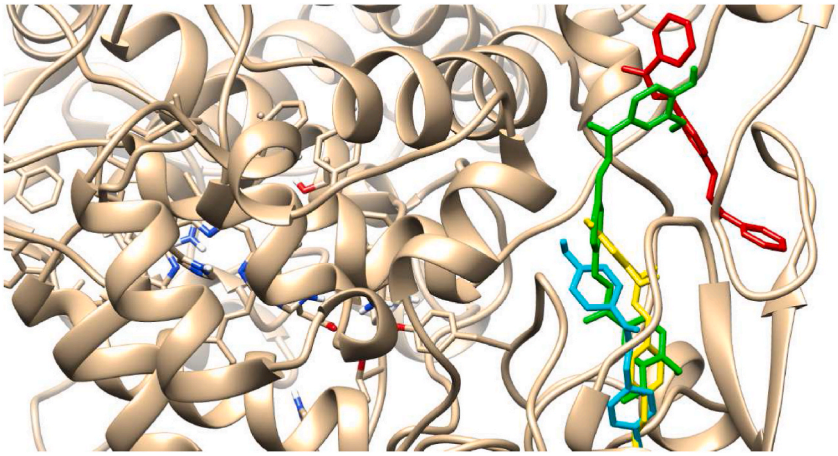

Fig. 12. Docked ligands: **3a** (red), **3b** (green), **3c** (yellow), **3d** (cyan); first poses; protein 3ln1.pdb. (For interpretation of the references to colour in this figure legend, the reader is referred to the Web version of this article.)

150.15°). Moreover, involving the MM/PB(GB)SA methods, we used the fastDRH server [43]. In the case of 3ln1.pdb, the Pro139 was selected as the hot-spot amino acid (Fig. D.4 in the Supplementary Materials) computed energy equalled: 2.400 kcal mol^{-1}) with the distance from the **3c** derivative ca. 3.00 Å. For a more detailed interaction analysis of ligand-amino acid, taking into account various

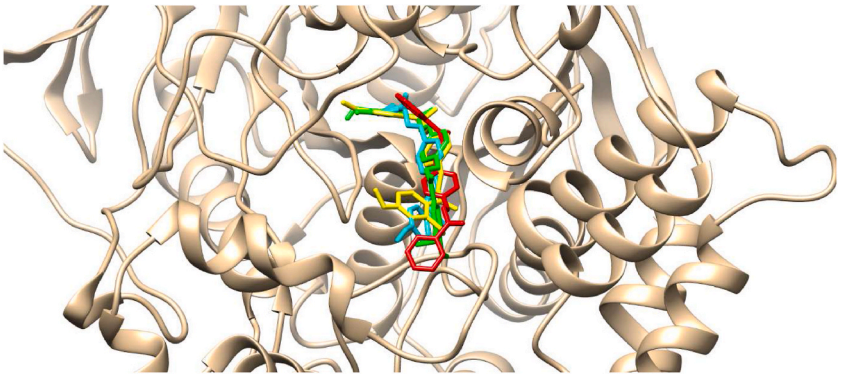

Fig. 13. Docked ligands: **3a** (red), **3b** (green), **3c** (yellow), **3d** (cyan); first poses; protein 3i6m.pdb. (For interpretation of the references to colour in this figure legend, the reader is referred to the Web version of this article.)

energy contributions, we used the SAPT approach, and the Psi4 1.3.2 software (Table D.2 in the Supplementary Materials) [44]. A detailed description using the SAPT0 approach is described in our previous investigations [45,46]. It also turned out that the lowest total SAPT0 energy was calculated for Gly30 (-10.846 kcal mol^{-1}) and Pro139 (-3.96672 kcal mol^{-1}), however the electrostatic type of contacts was beneficial for Gly30 (computed energy equalled -10.887 kcal mol^{-1}), and for Pro130 electrostatic term equalled barely -0.673 kcal mol^{-1}. Our data confirmed the assumptions originated from the *in vitro* experiments pointing the **3b** to be most active against the COX-2 protein.

Since chalcones were the subject of the *in vitro* test against their anticholinergic activity, compounds **3a**–**3d** were docked in the 3i6m.pdb protein [47]. In this case, the estimated binding affinity was as follows: 9.800, -11.100, -10.900, and -10.700 and -9.900 kcal mol^{-1} for derivatives **3a**–**3d** (Fig. 13), and **H0**, respectively. Surprisingly, the estimated binding affinity during the docking protocol of the **H0** was similar to the value computed for the chalcone **3a**. The computations using the fastDRH server and the MM/PB (GB)SA method (Fig. D.4 in the Supplementary Materials) pointed the Trp84 to be hot-spot (energy equalled: 2.060 kcal mol^{-1}) able to interact with **3b**. After docking protocol, we observed the following contacts formed between **3b** and particular amino acids, namely: C-H…O ($d = 2.590$ Å, $\theta = 171.70°$) for Trp84, O-H…O=C ($d = 2.637$ Å, $\theta = 88.74°$) for Tyr130, and O-H…O=C ($d = 2.602$ Å, $\theta = 105.53°$) and N-H…O ($d = 3.101$ Å, $\theta = 134.35°$) for Arg289. The observed distance between **3b** and Gly439 equalled ca. 1.9 Å, but no significant hydrogen bonds were detected in this case (Fig. D.3 in the Supplementary Materials). Moreover, for Trp84 was extracted the lowest total SAPT0 energy (-3.691 kcal mol^{-1}) with the corresponding computed value of the electrostatic term equalled -3.222 kcal mol^{-1} (Table D.2 in the Supplementary Materials). For Tyr130, the estimated energy of the electrostatic nature of contact was higher (only -0.093 kcal mol^{-1}) (see Fig. 14).

On this account, compound **3b** seems to be the most efficient for interaction with the *Torpedo californica* AChE in our model and the complex is stabilized by the hydrogen bonds formed within the cavity (Fig. D.2. in the Supplementary Materials). *In silico* analysis of interactions of the *bis*-chalcones investigated with the human BChE proved the most significant ability of compound 3a to form contacts within the cavity of the 1p0p.pdb target [48]. The computed binding energies were as follows: 9.400, -8.100, -8.900, and -9.200 and -7.900 kcal mol^{-1} for derivatives **3a**–**3d** (Fig. 13 and Fig. D.2. in the Supplementary material), and **H0**, respectively and the poor activity of analogue **3b** seemed to be originated from the fact that its docked pose is not similar to other derivatives. From the energetic standpoint, however, the **H0** analog was definitely not favourable. The computations using the fastDRH server (Fig. D.4 in the Supplementary Materials) allowed us to make an assumption that Trp82 seemed to be a hot-spot (energy equalled: 2.470 kcal mol^{-1}). We observed that the docked **3b** derivative was able to form the following contacts with particular amino acids as follows: N-H…O=C ($d = 3.084$ Å, $\theta = 90.99°$) for Trp82, and C-H…O=C ($d = 2.721$ Å, $\theta = 126.29°$) for Tyr332. The Gly439 was located in the proximity of ca. 1.9 Å with no significant contacts detected (Fig. D.3 in the Supplementary Materials). The lowest total SAPT0 energy was calculated for Tyr332 (-9.532 kcal mol^{-1}) with the corresponding computed value of the electrostatic term equalled -4.735 kcal mol^{-1} (Table D.2 in the Supplementary Materials). Surprisingly, for Trp82 electrostatic nature of contact with **3b** was much lower (-0.00021 kcal mol^{-1}).

Regarding the interactions of derivatives **3a**–**3d** with the aryl hydrocarbon receptor (PDB entry: 4m4x.pdb [49], the calculated binding affinity was as follows: 9.200, -7.200, -8.700, and -8.900 (Fig. 15 and Fig. D.2. in the Supplementary Materials), and -8.500 kcal mol^{-1} for derivatives **3a**–**3d**, and **H0**, respectively. The energies for **3c** and **3d** were similar to values resulting from the **H0** analog. This suggests that compound **3a** was able to interact within the cavity. The location of the docked pose of compound **3b** was, however, far different. The computations using the fastDRH server (Fig. D.4 in the Supplementary Materials) suggested that Leu10B might be a hot-spot (energy equalled: 2.880 kcal mol^{-1}) for interaction with **3a**, which seemed to be confirmed by SAPT0 energy calculations (the lowest values of total SAPT0 equalled: 4.567 and -3.115 kcal mol^{-1} for Leu110B and Tyr135B, respectively; Table D.2 in the Supplementary Materials). On the other hand, typical hydrogen bonds were not detected between **3a** and mentioned amino acids (Fig. D.3 in the Supplementary Materials).

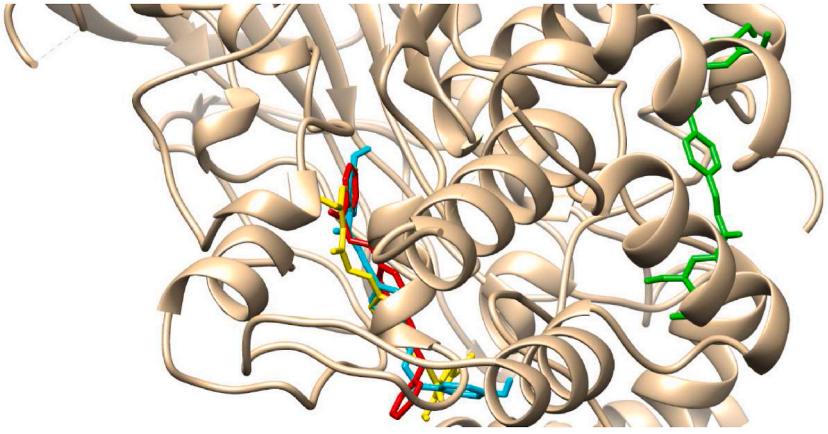

Fig. 14. Docked ligands: **3a** (red), **3b** (green), **3c** (yellow), **3d** (cyan); first poses; protein 1p0p.pdb. (For interpretation of the references to colour in this figure legend, the reader is referred to the Web version of this article.)

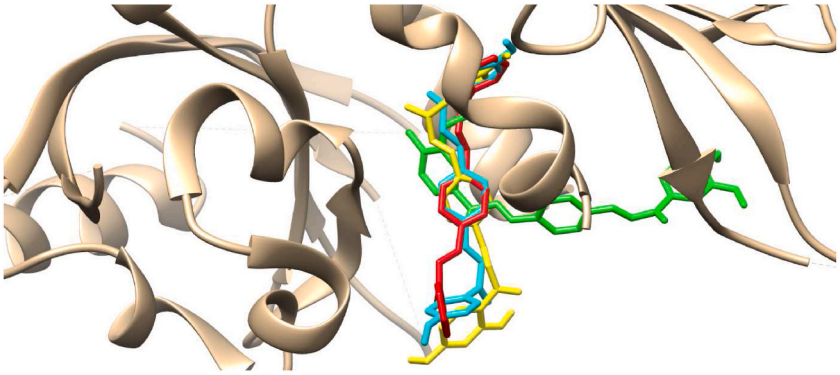

Fig. 15. Docked ligands: **3a** (red), **3b** (green), **3c** (yellow), **3d** (cyan); first poses; protein 4m4x.pdb. (For interpretation of the references to colour in this figure legend, the reader is referred to the Web version of this article.)

The chalcone **3b** seemed to be favored for interaction with the human PPAR-γ protein (2ath. pdb [47]) as its docking pose significantly differs from other analogs tested. In this model, the binding affinity was as follows: 7.200, −9.600, −7.500, and −8.300, and 7.300 kcal mol^{-1} for derivatives **3a**–**3d** (Fig. 16 and Fig. D.2. in the Supplementary Materials), and **H0**, respectively. It turned out that the energies for **3a** and **3c** were similar to values resulting from the **H0** analog. According to data taken from the computations using the fastDRH server and the MM/PB(GB)SA method (Fig. D.4 in the Supplementary Materials), Ile341 seemed to be a hot-spot (energy equalled: 1.970 kcal mol^{-1}) for interactions with **3b**, which was proved by the total SAPT0 interaction energy computations (Table D.2 in the Supplementary Materials) with the lowest values computed for: Ser342 (−3.497), Ile341 (−3.459), Leu330 (−3.311), and Cys285 (−2.783 kcal mol^{-1}). The electrostatic terms were as follows: 2.752, −3.006, −2.476, and −0.514 kcal mol^{-1} for Ser342, Ile341, Leu330, and Cys285, respectively. The distance to Glu272, Cys285, Leu330, and Ile341 equalled ca.: 3.2–3.7 Å, 3.1 Å, 3.3 Å, 2.8–3.5 Å, respectively, however typical hydrogen bonds were not observed within the ligand-amino acid complexes (Fig. D.3 in the Supplementary Materials). Only several types of contacts were detected, namely: N-H…O (d = 1.966 Å, θ = 155.90°) for: Gln273, C-H…O (d = 2.964 Å, θ = 111.52°) for Ser342 or O-H…O=C (d = 3.166 Å, θ = 82.61°) for Met364.

Based on the data extracted from the *in silico* models, we assume that our results correlated with the *in vitro* experiments, proving the expected activity of the most potent agents, namely **3a** (for interactions with the 4m4x.pdb and 1p0p.pdb proteins), **3b** (3i6m.pdb and 2ath.pdb) and **3c** (3ln1.pdb).

3. Structure-activity relationships

Comparing the effect on HORAC activity, *bis*-chalcone **3d**, containing two hydroxy groups in its structure, was the most active, but the introduction of two methoxy groups in position ortho to hydroxy groups (**3b**) resulted in a decrease in the capacity to block the fluorescent probe's radical hydroxyl oxidation.

Introducing electron-donating groups to the phenyl rings of *bis*-chalcone impacted the activity of antioxidant" enzymes. Isomeric compounds containing methoxy and hydroxy groups (**3b**, **3c**) decreased the activity of antioxidant enzymes GR, GPx, and CAT. Analog **3d** containing only two electron-donating groups (OH) decreased GPx activity only, but *bis*-chalcone **3a**, without substituents, negatively affected glutathione reductase and catalase activity. Also, introducing electron-donating groups into the *bis*-chalcone structure influenced the anti-inflammatory activity of the *bis*-chalcones tested. The derivatives that are isomers containing hydroxy

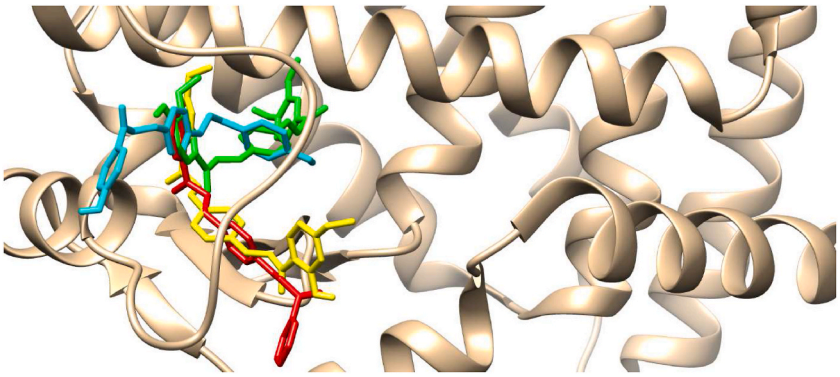

Fig. 16. Docked ligands: **3a** (red), **3b** (green), **3c** (yellow), **3d** (cyan); first poses; protein 2ath.pdb. (For interpretation of the references to colour in this figure legend, the reader is referred to the Web version of this article.)

and methoxy groups (**3b** and **3c**) showed a more significant ability to inhibit COX-2 than compound **3d,** containing only OH groups in both aromatic rings.

Investigation of the anti-AChE and anti-BChE effect of the four *bis*-chalcones tested indicated that the most significant inhibition of AChE was shown by compound **3b** with electron-donating groups (OCH_3) in the phenyl system of the *bis*-chalcone, a little less active was its isomer **3c**. Whereas *bis*-chalcones without substituents (**3a**) or with hydroxyl in the phenyl ring (**3d**) were more efficient against BChE than their analogs containing methoxy groups.

Resazurin reduction assay revealed that exposure of HT-22 cells to the derivatives containing hydroxyl and methoxyl in both aromatic systems (**3b**, **3c**) decreased resazurin levels. The compound not containing these substituents in its structure (**3a**) had the opposite effect, causing an increased cell metabolism or the number of cells. Similar relationships were revealed by LDH release. The compound **3a** without substituents did not affect the LDH release in HT-22 cells. Whereas, introducing methoxy and hydroxy groups to the phenyl rings resulted in the strong toxicity of these compounds, indicated by a decreased resazurin reduction test.

The *bis*-chalcones **3b** and **3c** obtained differ in the positions of the hydroxyl and methoxyl in both aromatic rings. Our protein expression analysis indicates that the action of isomer compounds may be opposite and proceed through different molecular pathways. Compound **3b** is likely to have pro-inflammatory properties because it decreases AhR and ARNT protein expression, PPARγ protein expression, and PPARγ coactivator and increases the amount of phosphorylated (p(S32)) IkBα protein expression. The isomeric compound **3c** increases AhR and ARNT protein level expression while decreasing PPARγ and its coactivator PGC-1α. Moreover, there causes an increase in NF-κB and IκBα levels. Therefore, compound **3c** does not initiate the inflammation process. Furthermore, our studies suggest that these two isomers act through different molecular pathways: compound **3b** works mainly through the PPARγ molecular pathway, while compound **3c** acts through the AhR pathway.

4. Conclusions

In conclusion, *bis*-chalcone type compounds (**3a-3d**) have been synthesized using the Claisen-Schmidt alkaline condensation method with aqueous NaOH solution (40 %) in ethanol at room temperature. These reactions run with good yields (79–88 %). Moreover, the by-products, monocondensation products containing a free aldehyde group, were confirmed. The structural identity of the products was characterized by spectroscopic methods such as ^{1}H and ^{13}C NMR, FT-IR, MS and UV–Vis. The high capacity of all four compounds tested to block the fluorescent probe's radical hydroxyl oxidation was estimated. The compound **3d** is characterized by high antioxidant capacity relative to the reference gallic acid. The derivatives containing OH groups could inhibit COX-2 with the most active compound **3c** and the substances tested can reduce the inflammatory response induced by COX-2. *Bis*-chalcones tested were evaluated as potential AChE and BChE inhibitors. The enzymes were inhibited by all compounds tested. All *bis*-chalcones were more efficient against BChE than AChE except compound **3b**, which showed the opposite effect. The most significant inhibition of BChE was shown by compound **3a**. The most significant inhibition of AChE was demonstrated by compound **3b**. *Bis*-chalcones' influence on the mouse hippocampal neuronal cell line (HT-22) was studied by resazurin reduction assay, LDH release and PGC-1α, PPARγ and GAPDH protein expression of compounds tested. Our data showed that in HT-22 cell line in the 50 and 100 μM, all studied compounds are toxic. Moreover, our data concerning AhR, ARNT, PGC-1α, PPARγ, p(S32)-IκBα, IκBα and NF-κB suggest that compounds **3a, 3c** and **3d** act through the AhR pathway, while compound **3b** works mainly through the PPARγ molecular pathway.

Moreover, the *in silico* method to evaluate the spectroscopic properties of analytes **3a**–**3d** was employed. Their geometry was previously optimized. Several descriptors related to HOMO–LUMO orbitals for compounds **3a–3d** were computed using water as the solvent for the simulation of the cell environment. For derivative **3b,** we noticed the lowest value of the chemical hardness (η). The present work showed that the highest value of the η parameter corresponded to *bis*-chalcone **3a**. As far as chemical potential was concerned, ligand **3a** revealed the most negative chemical potential value. The first excited state of the analytes corresponded to their λ_{max} value in the UV–Vis spectrum data. The calculated UV–Vis spectra showed compliance with the experimental ones with the use of PBE1PBE functional. Using an *in silico* approach, we discussed the interactions of *bis*-chalcones **3a**–**3d** with selected biological targets: aryl hydrocarbon receptor (AHR) PAS-A Domain, human PPARγ ligand binding domain, soman-aged human BChE in the complex with the substrate analogue butyrylthiocholine, *Torpedo californica* AChE complexed with N-piperidinopropyl-galanthamine, and the COX-2 active site complexed with celecoxib, acquired from the Protein Data Bank base. For this purpose, we also used the fastDRH server, the MM/PB(GB)SA, and the SAPT methods. Based on the data extracted from the *in silico* models, the **3a**, **3b** and **3c** chalcone analogs were deemed to be the most potent agents. Considering the obtained results and the significant activity of the obtained derivatives with a chalcone structure, especially those containing hydroxyl groups, it is intended to subject them to further biological tests, in particular for anticancer tests. Moreover, it is planned to further modify their structure and then assess and compare their biological properties.

5. Materials and methods

5.1. Solvents and chemicals

An aqueous solution of NaOH (40 %), terephthalaldehyde, acetophenone, apocynin, 2-hydroxy-4-methoxyacetophenon (paeonol), 4-hydroxyacetophenone (piceol) and solvents (ethanol, dichloromethane, ethyl acetate, n-hexane and DMSO) from Aldrich (Saint Louis, USA), Fluka (Buchs, Switzerland), Chempur (Piekary Śląskie, Poland), and POCh S.A. (Gliwice, Poland) were used.

All other chemicals of the highest purity were commercially available, and demineralized water was used in the tests.

5.2. Instrumental analysis

The melting points of all compounds obtained in this study were determined on a Boetius apparatus and were uncorrected. The Nicolet iS50 FT-IR spectrometer (Thermo Scientific, Waltham, Massachusetts, USA) was used to record the IR spectra. UV–Vis spectra were obtained using an uniSPEC 2, LLG spectrophotometer Labware. The NMR Varian VNMR-S 400 MHz spectrometer (Agilent Technologies, Santa Clara, CA, USA) was used to record the ^{1}H and ^{13}C NMR spectra (400 and 100 MHz, respectively). The chemical shifts were expressed in parts per million (ppm) relative to tetramethylsilane (TMS) as an internal standard, using DMSO-d_6 as the solvent. Coupling constants *(J)* are expressed in Hertz (Hz). Signals are labelled as follows: s, singlet; d, doublet; dd, double doublet; t, triplet; m, multiplet. The MS spectra were recorded on a Bruker 320MS/420 GC spectrometer apparatus (Bruker Corporation, Billerica, MA, USA) using the electron impact technique (EI), operating at 75 eV. The progress of the reactions and the purity of products were checked using the TLC method on silica gel plates (DC-Alufolien Kieselgel 60 F_{254} from Merck, Darmstadt, Germany). As the eluents, hexane and ethyl acetate (2:1, 4:3, 9:1, *v/v*) or chloroform and methanol (9:1, *v/v*) were used. The TLC spots on the plates were observed in UV light (λ = 254 nm). Silica gel 60 (63–200 μm particle size, Merck) was used for the column chromatography. The crystallization process or flash column chromatography with hexane and ethyl acetate (2:1, *v/v*) were used for the crude reaction products purified.

5.3. General procedure for the synthesis of bis-chalcones

5 mL of 40 % NaOH (an aqueous solution) was added dropwise into a solution of 6 mM of aromatic methylketone (acetophenone, apocynin, paeonol, piceol) in 20 mL of ethanol. Then, 3 mM of terephthalaldehyde in 5 mL of an ethanolic solution was added to the reaction mixture. The mixture was stirred for 48 h at room temperature and then poured into cold water with ice and neutralized with 10 % aqueous HCl until a precipitate formed. The solid obtained was filtered, washed with demineralized water, and crystallized (methanol) to yield the final crude compound. If no precipitate formed in an aqueous medium, extraction with dichloromethane was performed. The organic extraction layers were washed with 10 % aqueous HCl and then with demineralized water and dried over the anhydrous $MgSO_4$. Dichloromethane was removed using a vacuum evaporator. The solid was additionally purified by column chromatography method using chloroform:methanol (9:1, *v/v*) as an eluent.

5.3.1. (2E,2E)-3,3'-(1,4-phenylene)bis(1-phenylprop-2-en-1-one) **(3a)**

Yield: 88 %; white solid; R_f ($CHCl_3$:MeOH, 9:1) = 0.20; Mp = 180–183 °C (Mp = 191–193 °C [26]); UV–Vis: $^{MAX}\lambda_{(CHCl3)}$ = 393 nm, $^{MAX}\lambda_{MeOH}$ = 364 nm; FT-IR (υ cm^{-1}): 3052, 3037, 1653, 1604, 1583, 1444, 1334, 1222, 978, 832; 769; EI-MS, *m/z* (%): 338 (60) M^+, 309 (9), 253 (8), 233 (100), 202 (23), 178 (19), 104 (30), 77 (17); ^{1}H NMR (400 MHz, DMSO-d_6) (*δ*[ppm]): 8.20 (d, *J* = 7.20 Hz, 4H, ArH), 8.07 (d, *J* = 15.60 Hz, 2H, CH =), 8.01 (s, 4H, ArH), 7.80 (d, *J* = 15.60 Hz, 2H, CH =), 7.70 (t, *J* = 7.30 Hz, 2H, ArH), 7.60 (t, *J* = 7.60 Hz, 4H, ArH); ^{13}C NMR (DMSO-d_6) (*δ*[ppm]): 189.12 (2xC=O), 143.09 (2xCH), 137.47 (2xC), 136.69 (2xC), 133.28 (2xCH), 129.44 (4xCH), 128.83 (4xCH), 128.61(4xCH), 123.03 (2xCH).

5.3.2. (2E,2E)-3,3'-(1,4-phenylene)bis(1-(4-hydroxy-3-methoxyphenyl)prop-2-en-1-one **(3b)**

Yield: 79 %; yellow solid; R_f ($CHCl_3$:MeOH, 4:3) = 0.21; Mp = 170–171 °C; UV–Vis: $^{MAX}\lambda_{(CHCl3)}$ = 282 nm, $^{MAX}\lambda_{MeOH}$ = 233 nm; FT-IR (υ cm^{-1}): 3296, 2917, 2851, 1640, 1564, 1508, 1445, 1270, 1020, 976, 801, 753; EI-MS, *m/z* (%): 430 (34) M^+, 279 (25), 253 (8), 165 (33), 151 (100), 108 (20), 103 (34), 77 (7); ^{1}H NMR (400 MHz, DMSO-d_6) (*δ*[ppm]): 10.03 (s, 2H, OH), 8.05-7.97 (m, 1H, ArH), 7.91 (d, *J* = 15.60 Hz, 2H, CH =), 7.84 (d, *J* = 8.10 Hz, 4H, ArH), 7.79 (dd, *J* = 8.40, 2.00 Hz, 2H, ArH), 7.68 (d, *J* = 15.60 Hz, 2H, CH =), 7.62 (d, *J* = 2.00 Hz, 1H, ArH), 7.40 (d, *J* = 8.10 Hz, 2H, ArH), 6.91 (d, *J* = 8.30 Hz, 1H, ArH), 3.83 (s, 6H, 2xOCH_3); ^{13}C NMR (DMSO-d_6) (*δ*[ppm]): 187.00 (2xC=O), 151.89 (2xC), 147.75 (2xC), 145.14, 142.67, 133.29 (2xC), 129.46 (2xC), 128.60 (2xC), 126.69 (2xC), 123.67 (2xC), 121.32 (2xC), 114.97 (2xC), 111.60 (2xC), 55.69 (2xOCH_3).

5.3.3. (2E)-4-(3-(4-hydroxy-3-methoxyphenyl)-3-oxoprop-1-en-1-yl)benzaldehyde **(3bb)**

Yield: 15 %; light yellow solid; R_f ($CHCl_3$:MeOH, 4:3) = 0.60; Mp = 207–208 °C; FT-IR (υ cm^{-1}): 3206, 2917, 1640, 1565, 1508, 1418, 1270, 977, 801, 753; EI-MS, *m/z* (%): 284 (100) M+, 283 (43), 253 (84), 165 (33), 151 (93), 131 (40), 103(34), 77 (42).

5.3.4. (2E,2E)-3,3'-(1,3-phenylene)bis(1-(2-hydroxy-4-methoxyphenyl)prop-2-en-1-one **(3c)**

Yield: 83 %; yellow solid; R_f (hexane:ethyl acetate, 2:1) = 0.58; Mp = 150–151 °C; UV–Vis: $^{MAX}\lambda_{(CHCl3)}$ = 380 nm, $^{MAX}\lambda_{MeOH}$ = 375 nm; FT-IR (υ cm^{-1}): 3359, 2917, 2850, 1636, 1564, 1506, 1357, 1215, 957, 825, 798; EI-MS, *m/z* (%): 430 (30) M^+, 279 (12), 239 (4), 177 (49), 151 (100), 108 (17), 77 (10); ^{1}H NMR (400 MHz, DMSO-d_6) (*δ*[ppm]): 10.06 (s, 2H, OH), 8.32 (d, *J* = 9.10 Hz, 1H, ArH), 8.19 (d, *J* = 15.50 Hz, 2H, CH =), 8.15 (d, *J* = 8.30 Hz, 1H, ArH), 7.99 (d, *J* = 8.30 Hz, 4H, ArH), 7.88 (d, *J* = 15.50 Hz, 2H, CH =), 6.60 (dd, *J* = 9.00, 2.50 Hz, 2H, ArH), 6.55 (d, *J* = 2.50 Hz, 2H, ArH), 3.87 (s, 6H, 2xOCH_3); ^{13}C NMR (100 MHz, DMSO-d_6) (*δ*[ppm]): 192.63 (2xC=O), 166.23, 165.72, 142.29, 140.11, 137.05, 132.88, 129.82, 129.55, 124.33, 113.93, 107.58, 100.94, 55.81 (2xOCH_3).

5.3.5. (2E)-4-(3-(2-hydroxy-4-methoxyphenyl)-3-oxoprop-1-en-1-yl)benzaldehyde **(3cc)**

Yield: 10 %; yellow solid; R_f (hexane:ethyl acetate, 2:1) = 0.27; Mp 78–79 °C; FT-IR (υ cm^{-1}): 3359, 2917, 2850, 1636, 1564, 1506, 1444, 1357, 1276, 1195, 11276, 1015, 955, 857, 873, 860, 798; EI-MS, *m/z* (%): 282 (47) M^+, 281 (32), 266 (30), 238 (6), 177 (100), 151 (61), 122 (16), 103 (20), 77 (24).

5.3.6. (2E,2E)-3,3-(1,4-phenylene)bis(1-(4-hydroxyphenyl)prop-2-en-1-one ***(3d)***

Yield: 85 %, yellow solid; R_f ($CHCl_3$:MeOH, 9:1) = 0.51; Mp 227–229 °C; UV–Vis: $^{MAX}\lambda_{(CHCl3)}$ = 328 nm, $^{MAX}\lambda_{MeOH}$ = 379 nm; FT-IR (υ cm^{-1}): 3426, 3152, 2950, 1637, 1602, 1587, 1545, 1510, 1342, 1225, 973, 820, 752; EI-MS, *m/z* (%): 370 (53) M^+, 341 (10); 249 (100); 223 (31); 202 (12), 121 (91); 93 (13); ^{1}H NMR (400 MHz, DMSO-d_6) (δ[ppm]): 10.45 (s, 2H), 8.10 (d, *J* = 8.70 Hz, 4H, ArH), 8.00 (d, *J* = 15.60 Hz, 2H, CH =), 7.96 (s, 4H, ArH), 7.71 (d, *J* = 15.60 Hz, 2H, CH =), 6.93–6.90 (m, 4H, ArH); ^{13}C NMR (100 MHz, DMSO-d_6) (δ[ppm]): 187.01(2xC=O), 162.25 (2xC), 141.80 (2xCH), 136.61 (2xC), 131.22 (2xC), 129.15 (4xCH), 129.03 (4xCH), 123.00 (2xCH), 115.37 (2xCH), 102.03 (2xC).

5.3.7. 4-(3-(4-hydroxy-3-metoxyphenylo)-3-oxoprop-1-en-1-ylo)benzaldehyde ***(3dd)***

Yield: 11 %, light orange solid; R_f ($CHCl_3$:MeOH, 9:1) = 0,64; Mp 165–166 °C; EI-MS, *m/z* (%): 284 (100) M^+, 283 (43), 253 (84), 165 (33), 151 (93), 131 (40), 103 (28), 77(34), 77 (42).

5.4. Biological study

5.4.1. Estimation of an antioxidant, anti-inflammatory and anti-neurodegenerative activity

5.4.1.1. Preparation of samples. Samples were dissolved in DMSO (Sigma D4540) to obtain a 3 mM/dm^3 concentration.

5.4.1.2. HORAC. Analysis was performed as described in Szwajgier et al. [50]. The samples were prepared at a concentration of 1 mg/mL DMSO. The only modification was that the volumes of all reagents used for the measurements were reduced 4-fold (proportionally) to measure the absorbance using a microplate reader (Varioskan Lux, Thermo Scientific).

5.4.1.3. Effect on GPx and GR activity. The analyses were performed exactly as described in Studzińska-Sroka et al. [51].

5.4.1.4. Effect on CAT activity. Watanabe et al. method [52] was used with the following modifications. The reaction mixture was composed of: 0.02 mL EDTA solution (56.5 mM), 0.01 mL sample, 0.02 mL 3 % H_2O_2 solution (Sigma H1009), 0.02 mL catalase solution (4000-fold diluted, Sigma C3515) (all reagents except tested sample were diluted in TRIS buffer, pH 7.0, 1 M). The volume was completed to 0.31 mL with the same buffer solution. DMSO (Sigma D4540) replaced the tested sample in a blank sample. The background of the sample was measured in a mixture composed of 0.01 mL sample completed to 0.31 mL by the buffer. The absorbance was read at 240 nm directly after the mixing and after 5 min of incubation (room temperature). The decrease of absorbance (depletion of H_2O_2) in the tested and blank samples was compared. The calibration curve was produced using eleven H_2O_2 solutions (0.5693–5.693 mM/dm^3). The results are expressed in % inhibition and as H_2O_2 depletion (mM depleted H_2O_2/dm^3 min).

5.4.1.5. Effect on COX-2 activity. The analysis was performed exactly as described in Studzińska-Sroka et al. [51], except that the volume of the samples tested added to the reaction mixture was 0.02 mL.

Inhibition of the enzyme activity was expressed in % (indicates by how many % the activity has been reduced in relation to the negative or blank sample for which the maximum activity was assumed as 100 %, under the conditions used in the method). Moreover, inhibition of enzyme activity was expressed as acetylsalicylic acid equivalent concentration (mg/mL).

5.4.1.6. Effect on AChE and BChE activity. The analysis was performed exactly as described in Studzińska-Sroka et al. [51], except that the volume of the samples tested added to the reaction mixture was 0.035 mL.

5.4.2. The mouse hippocampal neuronal cell line (HT-22) study

5.4.2.1. Sample preparation. The 1000x-STOCKs of compounds **3a, 3b, 3c** or **3d** were obtained by dissolving specific portions of these compounds in appropriate volumes of pure, sterile DMSO. Subsequently, the dilution of the substances tested was performed directly in the medium. Thus, the total amount of DMSO didn't exceed 0.1 %.

5.4.2.2. Cell culture. Dr P. Sołek kindly gifted the mouse hippocampal neuronal cell line (HT-22, RRID: CVCL_0321, Sigma-Aldrich, cat. SCC129). The cells were cultured in phenol red-free DMEM with 10 % FBS and 0.1 % penicillin/streptomycin until reaching an 80 %-confluency. After this, the cells were trypsinized and seeded at the density of 4×10^3 cells/well or 2×10^5 cells/well in 96-well plates (resazurin reduction and LDH release assays) or 6-well plates (Western Blot), respectively. Subsequently, the cells were subcultured for 24h, followed by treatment with compounds **3a, 3b, 3c,** or **3d** (concentrations described in a specific methodology below).

5.4.2.3. Resazurin reduction assay. The method was performed as described earlier [53]. HT-22 cells were treated with compounds **3a, 3b, 3c,** or **3d** in the concentration range between 1 nM–100 μM, dissolved in the growth medium (DMEM with 10 % of FBS) for 24 h and 48 h. After a specific interval, the medium was removed and replaced with a staining mix containing 10 % resazurin sodium salt and 0.1 % FBS in DMEM for 1h. Subsequently, the fluorescence intensity was measured at an excitation wavelength equal to 570 nm and an emission wavelength equal to 590 nm using a microplate reader (FilerMax F5, Molecular Devices, San Jose, USA). The results were expressed as percentages (%) relative to the control (DMSO-treated cells).

5.4.2.4. LDH release assay. The LDH release assay was performed according to the producer's manual (Takara Bio, Kusatstu, Japan). The cells were treated with certain concentrations of compounds **3a, 3b, 3c** or **3d**, and next, the medium was transferred to a new 96-well plate. Simultaneously, the staining solution was prepared by mixing the dye solution with the catalyst (1:45, *v/v* ratio). Next, the obtained liquid was added to each well, and the plates were incubated in the dark for 30 min in RT. Then, the absorbance was measured at a wavelength equal to 450 nm. The results were expressed as percentages (%) of the control (DMSO-treated cells).

5.4.2.5. Western Blot. The method was carried out as described previously with some modifications [54]. HT-22 cells were treated with 10 μM of compounds **3a, 3b, 3c** or **3d** for 24 h. Then, the medium was removed, cells were washed once with PBS, and the lysates were collected using RIPA buffer. Subsequently, the protein concentration was measured and standardized using the BCA method – BSA was used as a standard [55]. Next, the samples were separated by an SDS-PAGE electrophoresis using 7.5 % acrylamide/bisacrylamide gel. Subsequently, the protein was transferred to a PVDF membrane (pore size: 0.45 μm) overnight at 30 V, at 4 °C. After this, the non-specific side blocking was performed, using 1 % BSA in TBST for 1h, followed by an incubation of the membranes with specific primary antibodies: PGC-1α, PPARγ, p(S32)-IκBα, IκBα, ARNT, SOD1, AhR, NF-κB and GAPDH in 4 °C, overnight. On the next day, the membranes were washed 3-time for 10 min in TBST, followed by the secondary HRP-conjugated anti-mouse or anti-rabbit antibodies for 1h at room temperature. Next, the membranes were washed three times with TBST and once in TBS, followed by an ECL-based detection. The GAPDH protein expression was always used as a loading control (after stripping the membrane). The band's intensity was measured using GelQuantNET software – each measurement was performed three times. The raw blots were added in the Supplementary Materials.

5.4.2.6. Statistical analyses. The data was presented as means with standard deviations (SD) of at least three replicates ($n \geq 3$). The one-way analyses of variance (ANOVA) with Tuckey's post-hoc test were performed using Statistical Mode in GraphPad Prism 8.0 software. The data denoted as *, ** and *** are statistically different compared to the control at $p < 0.05$, $p < 0.01$ and $p < 0.001$, respectively.

5.5. Computational studies

The structures of compounds tested **3a–3d** were initially optimized (Gaussian 16C.01 program [41]) using DFT formalism, namely: (a) B3LYP/6-31G(d,p) [56], (b) PBE1PBE/6-31G(d,p) [57,58] approaches. For HOMO–LUMO orbitals and UV–vis calculations, we applied the functional/6–311++G(2d,3p) approximation (TD-DFT method), the integral equation formalism variant (IEFPCM), the linear response (LR) approach, and: chloroform, methanol, and water as the solvents. The HOMO–LUMO orbitals for the compounds were extracted with *GaussView 5.0* program [59] using checkpoint files. We used the Gabedit 2.3.4 software [60] with default settings for the analysis of theoretical UV–vis spectra. The structure of: aryl hydrocarbon receptor (AHR) PAS-A domain, ligand binding domain of human PPAR-γ, soman-aged human BChE in the complex with the substrate analogue butyrylthiocholine, *Torpedo californica* AChE complexed with N-piperidinopropyl-galanthamine, and the COX-2 active site complexed with celecoxib, taken from the Protein Data Bank base (PDB entries: 4m4x with the resolution of 2.55 Å, 2ath with the resolution of 2.28 Å, 1p0p with the resolution of 2.30 Å, 3i6m with the resolution of 2.26 Å, and 3ln1 with the resolution of 2.40 Å, respectively), were selected as the biological targets [37,38,47–49,61,62]. An initial targets for further optimization were prepared by removing the internal ligands from the 3i6m.pdb and 3ln1.pdb files but keeping the internal coordinates unchanged. The genetic algorithm (GA) method as implemented in the program AutoDock Vina [42], was employed for docking protocol. All water molecules and internal ligands were removed from the original PDB files. Polar hydrogen atoms were added, and partial charges were assigned to the protein. In the next step, the internal ligand was replaced by the optimized structure of investigated compounds 3a–3d, and additionally, the residues were saturated with hydrogen atoms. A grid box was defined to be of 70 Å size (coordinates: centre _x = 16.134, 14.946, 134.697, 3.776, and 30.953; centre_y = −2.696, 6.343, 121.618, 66.608, and −22.301; centre_z = 6.236, 35.674, 37.569, 65.866, and −16.833 for the 4m4x.pdb, 2ath.pdb, 1p0p.pdb, 3i6m.pdb, and 3ln1.pdb proteins, respectively). For each of all ligands the docking procedure was repeated 10 times, and the total overlap of resulted in docked poses was achieved in comparison with the geometry of internal ligands. For targets without internal ligand, the docking approach was repeated until the total overlap of resulted in docked poses was observed, and then rerun 10 times to prove if the total overlap of resulted in docked poses was maintained. The results of the docking procedure were visualized using the *Chimera 1.13.1* package [63] and *LigPlot + v.2.2* software [64,65]. For the MM/PB(GB)SA computations, we applied the fastDRH server [43]. For the SAPT (symmetry-adapted perturbation theory) approach (SAPT0 method) we used the Psi4 1.3.2 software (Table D.2 in the Supplementary Materials) [44], treating the complexes ligand-amino acid as a closed-shell system and utilizing the recommended jun-cc-pVDZ basis set. A detailed description using the SAPT0 approach is described in our previous investigations [45,46].

Institutional review board statement

Not applicable.

Informed consent statement

Not applicable.

Data availability statement

Data associated with our study has not been deposited into a publicly available repository and data will be made available on request.

CRediT authorship contribution statement

Dorota Olender: Writing – review & editing, Writing – original draft, Project administration, Methodology, Investigation, Conceptualization. **Jacek Kujawski:** Writing – review & editing, Formal analysis. **Bartosz Skóra:** Investigation. **Ewa Baranowska-Wójcik:** Investigation. **Katarzyna Sowa-Kasprzak:** Investigation. **Anna Pawełczyk:** Funding acquisition. **Lucjusz Zaprutko:** Supervision. **Dominik Szwajgier:** Writing – review & editing, Investigation. **Konrad A. Szychowski:** Writing – review & editing, Investigation.

Declaration of competing interest

The authors declare that they have no known competing financial interests or personal relationships that could have appeared to influence the work reported in this paper.

Acknowledgements

This research did not receive any specific grant from funding agencies in the public, commercial, or not-for-profit sectors.

Appendix A. Supplementary data

Supplementary data to this article can be found online at https://doi.org/10.1016/j.heliyon.2024.e37147.

References

[1] M.A. Soobrattee, V.S. Neergheen, A. Luximon-Ramma, O.I. Aruoma, T. Bahorun, Phenolics as potential antioxidant therapeutic agents: mechanism and actions, Mutat. Res. 11 (579) (2005) 200–213. https://doi:10.1016/j.mrfmmm.2005.03.023.
[2] D. Szwajgier, E. Baranowska-Wójcik, W. Kukula-Koch, K. Kowalik, M. Polak-Berecka, A. Waśko, Evolution of the anticholinesterase, antioxidant, and anti-inflammatory activity of Epilobium angustifolium L. infusion during in vitro digestion, J. Funct.Foods 85 (2021) 104645, https://doi.org/10.1016/j.jff.2021.104645.
[3] N. Moussa, N. Dayoub, Exploring the role of COX-2 in Alzheimer's disease: potential therapeutic implications of COX-2 inhibitors, Saudi Pharm. J. 31 (2023) 101729, https://doi.org/10.1016/j.jsps.2023.101729.
[4] E. Baranowska-Wójcik, D. Szwajgier, Alzheimer's disease: review of current nanotechnological therapeutic strategies, Expert Rev. Neurother. (2020), https://doi.org/10.1080/14737175.2020.1719069.
[5] C. Zhuang, W. Zhang, C. Sheng, W. Zhang, C. Xing, Z. Miao, Chalcone: a privileged structure in medicinal chemistry, Chem. Rev. 117 (2017) 7762–7810, https://doi.org/10.1021/acs.chemrev.7b00020.
[6] T. Constantinescu, C.N. Lungu, Anticancer activity of natural and synthetic chalcones, Int. J. Mol. Sci. 22 (2021) 11306, https://doi.org/10.3390/ijms222111306.
[7] P. Thapa, S.P. Upadhyay, W.Z. Suo, V. Singh, P. Gurung, E. Seok Lee, R. Sharma, M. Sharma, Chalcone and its analogs: therapeutic and diagnostic applications in Alzheimer's disease, Bioorg. Chem. 108 (2021) 104681, https://doi.org/10.1016/j.bioorg.2021.104681.
[8] X. Zhang, K.P. Rakesh, S.N.A. Bukhari, M. Balakrishna, H.M. Manukumar, H.L. Qin, Multi-targetable chalcone analogs to treat deadly Alzheimer's disease: current view and upcoming advice, Bioorg. Chem. 80 (2018) 86–93, https://doi.org/10.1016/j.bioorg.2018.06.009.
[9] Z. Rozmer, P. Perjesi, Naturally occurring chalcones and their biological activities, Phytochem. Rev. 15 (2016) 87–120, https://doi.org/10.1007/s11101-014-9387-8.
[10] Y. Ouyang, J. Li, X. Chen, X. Fu, S. Sun, Q. Wu, Chalcone derivatives: role in anticancer therapy, Biomolecules 11 (2021) 894, https://doi.org/10.3390/biom11060894.
[11] G. George, V.P. Koyiparambath, S. Sukumaran, A.S. Nair, L.K. Pappachan, A.G. Al-Sehemi, H. Kim, B. Mathew, Structural modifications on chalcone framework for developing new class of cholinesterase inhibitors, Int. J. Mol. Sci. 23 (2022) 3121, https://doi.org/10.3390/ijms23063121.
[12] A. Hasan, K.M. Khan, M. Sher, G.M. Maharvi, S.A. Nawaz, M.I. Choudhary, Atta-Ur-Rahman, C.T. Supuran, Synthesis and inhibitory potential towards acetylcholinesterase, butyrylcholinesterase and lipoxygenase of some variably substituted chalcones, J. Enzyme Inhib. Med. Chem. 20 (1) (2005) 41–47, https://doi.org/10.1080/14756360400015231.
[13] D. Olender, K. Sowa-Kasprzak, A. Pawełczyk, B. Skóra, L. Zaprutko, K.A. Szychowski, Curcuminoid chalcones: synthesis and biological activity against the human colon carcinoma (Caco-2) cell line, Curr. Med. Chem. 31 (33) (2024) 5397–5416. https://doi:10.2174/0109298673257972230919055832.
[14] D. Olender, M. Józkowiak, H. Piotrowska-Kempisty, K. Sowa-Kasprzak, L. Zaprutko, I. Muszalska-Kolos, E. Baranowska-Wójcik, D. Szwajgier, Curcuminoid chalcones; synthesis, stability, new neuroprotective and sonosensitizing activity, Pharmaceuticals 16 (2023) 1331, https://doi.org/10.3390/ph16091331.
[15] R. Pereira, A.M.S. Silva, D. Ribeiro, V.L.M. Silva, E. Fernandes, Bis-chalcones: a review of synthetic methodologies and anti-inflammatory effects, Eur. J. Med. Chem. 252 (2023) 115280, https://doi.org/10.1016/j.ejmech.2023.115280.
[16] V.J. Ram, A.S. Saxena, S. Srivastava, S. Chandra, Oxygenated chalcones and bischalcones as potential antimalarial agents, Bioorganic Med. Chem. Lett. 10 (2000) 2159–2161, https://doi.org/10.1016/S0960-894X(00)00409-1.
[17] S. Burmaoglu, A. Gobek, B.O. Aydin, E. Yurtoglu, B.N. Aydin, G.Y. Ozkat, Design, synthesis and biological evaluation of novel bischalcone derivatives as potential anticancer agents, Bioorg. Chem. 111 (2021) 104882, https://doi.org/10.1016/j.bioorg.2021.104882.
[18] M. Vijaya Bhaskar Reddy, Y.-C. Shen, E. Ohkoshi, K.F. Bastow, K. Qian, K.-H. Lee, Bis-chalcone analogues as potent NO production inhibitors and as cytotoxic agents, Eur. J. Med. Chem. 47 (2012) 97–103, https://doi.org/10.1016/j.ejmech.2011.10.026.

[19] B. Jiang, F. Han, M.-H. Lu, Z.-P. Wang, W. Liu, Y.-X. Zhang, Bis-chalcone polyphenols with potential preventive and therapeutic effects on PD: design, synthesis and in vitro disaggregation activity against α-synuclein oligomers and fibrils, Eur. J. Med. Chem. 239 (2022) 114529, https://doi.org/10.1016/j.ejmech.2022.114529.

[20] C.-Y. Cai, L. Rao, Y. Rao, J.-X. Guo, Z.-Z. Xiao, J.-Y. Cao, Analogues of xanthones - chalcones and bis-chalcones as α-glucosidase inhibitors and anti-diabetes candidates, Eur. J. Med. Chem. 130 (2017) 51–59, https://doi.org/10.1016/j.ejmech.2017.02.007.

[21] A. Modzelewska, C. Pettit, G. Achanta, N.E. Davidson, P. Huang, S.R. Khan, Anticancer activities of novel chalcone and bis-chalcone derivatives, Bioorg. Med. Chem. 15 (14) (2006) 3491–3495. https://doi:10.1016/j.bmc.2006.01.003.

[22] A. Sharma, B. Chakravarti, M. Prasad Gupt, J.A. Siddiqui, R. Konwar, R.P. Tripathi, Synthesis and anti breast cancer activity of biphenyl based chalcones, Bioorg. Med. Chem. 18 (13) (2010) 4711–4720, https://doi.org/10.1016/j.bmc.2010.05.015.

[23] E.M. Fathi, F.M. Sroor, K.F. Mahrous, M.F. Mohamed, K. Mahmoud, M. Emara, A.H.M. Elwahy, I.A. Abdelhamid, Design, synthesis, in silico and in vitro anticancer activity of novel bis-furanyl-chalcone derivatives linked through alkyl spacers, ChemistrySelect 6 (2021) 6202–6211, https://doi.org/10.1002/slct.202100884.

[24] J. Yang, W.W. Mu, G.Y. Liu, Synthesis and evaluation of the anticancer activity of bischalcone analogs in human lung carcinoma (A549) cell line, Eur. J. Pharmacol. 5 (2020) 173396. https://doi:10.1016/j.ejphar.2020.173396.

[25] T. Liargkova, D.J. Hadjipavlou-Litina, C. Koukoulitsa, E. Voulgari, C. Avgoustakis, Simple chalcones and bis-chalcones ethers as possible pleiotropic agents, J. Enzyme Inhib. Med. Chem. 31 (2) (2016) 302–313. https://doi:10.3109/14756366.2015.1021253.

[26] E. Polo, N. Ibarra-Arellano, L. Prent-Penaloza, A. Morales-Bayuelo, J. Henao, A. Galdamez, Ultrasound-assisted synthesis of novel chalcone, heterochalcone and bis-chalcone derivatives and the evaluation of their antioxidant properties and as acetylcholinesterase inhibitors, Bioorg. Chem. 90 (2019) 103034, https://doi.org/10.1016/j.bioorg.2019.103034.

[27] M.C. Díaz Flaqué, M.F. Cayrol, H.A. Sterle, M. Del Rosario Aschero, J.A. Díaz Albuja, B. Isse, R.N. Farías, L. Cerchietti, C. Rosemblit, G.A. Cremaschi, Thyroid hormones induce doxorubicin chemosensitivity through enzymes involved in chemotherapy metabolism in lymphoma T cells, Oncotarget 10 (32) (2019) 3051–3065, https://doi.org/10.18632/oncotarget.26890.

[28] S. Van den Bossche, E. Vandeplassche, L. Ostyn, T. Coenye, A. Crabbé, Bacterial interference with lactate dehydrogenase assay leads to an underestimation of cytotoxicity, Front. Cell. Infect. Microbiol. 10 (2020) 494, https://doi.org/10.3389/fcimb.2020.00494.

[29] M. Choudhary, G. Malek, The aryl hydrocarbon receptor: a mediator and potential therapeutic target for ocular and non-ocular neurodegenerative diseases, Int. J. Mol. Sci. 21 (18) (2020) 6777, https://doi.org/10.3390/ijms21186777.

[30] T. Liu, L. Zhang, D. Joo, S.C. Sun, NF-κB signaling in inflammation, Signal Transduct. Target. Ther. 2 (1) (2017) 1–9, https://doi.org/10.1038/sigtrans.2017.23.

[31] A.K. Wójtowicz, K.A. Szychowski, A. Wnuk, M. Kajta, Dibutyl phthalate (DBP)-induced apoptosis and neurotoxicity are mediated via the aryl hydrocarbon receptor (AhR) but not by estrogen receptor alpha (ERα), estrogen receptor beta (ERβ), or peroxisome proliferator-activated receptor gamma (PPARγ) in mouse cortical neurons, Neurotox. Res. 31 (2017) 77–89, https://doi.org/10.1007/s12640-016-9665-x.

[32] J. Korbecki, R. Bobiński, M. Dutka, Self-regulation of the inflammatory response by peroxisome proliferator-activated receptors, Inflamm. Res. 68 (2019) 443–458, https://doi.org/10.1007/s00011-019-01231-1.

[33] Z.X. Chong, C.Y. Yong, A.H.K. Ong, S.K. Yeap, W.Y. Ho, Deciphering the roles of aryl hydrocarbon receptor (AHR) in regulating carcinogenesis, Toxicology (2023) 153596, https://doi.org/10.1016/j.tox.2023.153596.

[34] T. Koopmans, Über die Zuordnung von Wellenfunktionen und Eigenwerten zu den Einzelnen Elektronen Eines Atoms, Physica 1 (1934) 104–113, https://doi.org/10.1016/S0031-8914(34)90011-2.

[35] D.A. Zainuri, I.A. Razak, S. Arshad, Molecular structure, DFT studies and UV–Vis absorption of two new linear fused ring chalcones: (E)-1-(anthracen-9-yl)-3-(2-methoxyphenyl)prop-2-en-1-one and (E)-1-(anthracen-9-yl)-3-(3-fluoro-4-methoxyphenyl)prop-2-en-1-one, Acta Cryst E74 (2018) 1087–1092, https://doi.org/10.1107/S205698901800974X.

[36] V.A. Adole, DFT calculations on three 2,3-dihydrobenzofuran linked chalcones: structural, HOMO-LUMO and spectroscopic (UV-Vis and IR) interpretation, Vietnam J. Chem. 61 (2) (2023) 147–157, https://doi.org/10.1002/vjch.202100023.

[37] R.A. Shinde, V.A. Adole, B.S. Jagdale, Antimicrobial and computational investigation of two 2,3-dihydro-1H-inden-1-one derived fluorinated chalcone motifs, Vietnam J. Chem. 59 (6) (2021) 800–812, https://doi.org/10.1002/vjch.202100028.

[38] S. Omar, M. Shkir, M.A. Khan, Z. Ahmad, S. AlFaify, A comprehensive study on molecular geometry, optical, HOMO-LUMO, and nonlinear properties of 1,3-diphenyl-2-propen-1-ones chalcone and its derivatives for optoelectronic applications: a computational approach, Optik 204 (2020) 164172, https://doi.org/10.1016/j.ijleo.2020.164172.

[39] J.L. Wang, D. Limburg, M.J. Graneto, J. Springer, J.R. Hamper, S. Liao, J.L. Pawlitz, R.G. Kurumbail, T. Maziasz, J.J. Talley, J.R. Kiefer, J. Carter, The novel benzopyran class of selective cyclooxygenase-2 inhibitors. Part 2: the second clinical candidate having a shorter and favorable human half-life, Bioorg. Med. Chem. Lett. 20 (2010) 7159–7163, https://doi.org/10.1016/j.bmcl.2010.07.054.

[40] B.K. Çavuşoğlu, B.N. Sağlık, U.A. Çevik, D. Osmaniye, S. Levent, Y. Özkay, Z.A. Kaplancıklı, Design, synthesis, biological evaluation, and docking studies of some novel chalcones as selective COX-2 inhibitors, Arch. Pharm. (2020) e2000273, https://doi.org/10.1002/ardp.202000273.

[41] Gaussian 16 rev. C.01/C.02 release notes | Gaussian.com. https://gaussian.com/relnotes/. (Accessed 2 May 2024).

[42] O. Trott, A.J. Olson, AutoDock Vina: improving the speed and accuracy of docking with a new scoring function, efficient optimization, and multithreading, J. Comput. Chem. 31 (2) (2010) 455–461, https://doi.org/10.1002/jcc.21334.

[43] Z. Wang, H. Pan, H. Sun, Y. Kang, H. Liu, D. Cao, T. Hou, fastDRH: a webserver to predict and analyze protein-ligand complexes based on molecular docking and MM/PB(GB)SA computation, Brief Bioinform 23 (5) (2022) bbac201, https://doi.org/10.1093/bib/bbac201.

[44] R.M. Parrish, L.A. Burns, D.G.A. Smith, A.C. Simmonett, A.E. DePrince III, E.G. Hohenstein, U. Bozkaya, A.Y. Sokolov, R. Di Remigio, R.M. Richard, J. F. Gonthier, A.M. James, H.R. McAlexander, A. Kumar, M. Saitow, X. Wang, B.P. Pritchard, P. Verma, H.F. Schaefer III, K. Patkowski, R.A. King, E.F. Valeev, F. A. Evangelista, J.M. Turney, T.D. Crawford, C.D. Sherrill, Psi4 1.1: an open-source electronic structure program emphasizing automation, advanced libraries, and interoperability, J. Chem. Theory Comput. 13 (7) (2017) 3185–3197, https://doi.org/10.1021/acs.jctc.7b00174. (Accessed 20 July 2024).

[45] K. Czaja, J. Kujawski, P. Śliwa, R. Kurczab, R. Kujawski, A. Stodolna, A. Myślińska, M.K. Bernard, Theoretical investigations on interactions of arylsulphonyl indazole derivatives as potential ligands of VEGFR2 kinase, Int. J. Mol. Sci. 21 (13) (2020) 4793, https://doi.org/10.3390/ijms21134793.

[46] P. Kobylka, M. Kucinska, J. Kujawski, D. Lazewski, M. Wierzchowski, M. Murias, Resveratrol analogues as selective estrogen signaling pathway modulators: structure–activity relationship, Molecules 27 (20) (2022) 6973, https://doi.org/10.3390/molecules27206973.

[47] N. Mahindroo, C.-F. Huang, Y.-H. Peng, C.-C. Wang, C.-C. Liao, T.-W. Lien, S.K. Chittimalla, W.-J. Huang, C.-H. Chai, E. Prakash, C.-P. Chen, T.-A. Hsu, C.-H. Peng, I.-L. Lu, L.-H. Lee, Y.-W. Chang, W.-C. Chen, Y.-C. Chou, C.-T. Chen, C.M.V. Goparaju, Y.-S. Chen, S.-J. Lan, M.-C. Yu, X. Chen, Y.-S. Chao, S.-Y. Wu, H.-P. Hsieh, Novel indole-based peroxisome proliferator-activated receptor agonists: design, SAR, structural biology, and biological activities, J. Med. Chem. 48 (2005) 8194–8208, https://doi.org/10.1021/jm0506930.

[48] Y. Nicolet, O. Lockridge, P. Masson, J.C. Fontecilla-Camps, F. Nachon, Crystal structure of human butyrylcholinesterase and of its complexes with substrate and products, J. Biol. Chem. 278 (2003) 41141–41147, https://doi.org/10.1074/jbc.M210241200.

[49] D. Wu, N. Potluri, Y. Kim, F. Rastinejad, Structure and dimerization properties of the aryl hydrocarbon receptor PAS-A domain, Mol. Cell Biol. 33 (2013) 4346–4356, https://doi.org/10.1128/MCB.00698-13.

[50] D. Szwajgier, E. Baranowska-Wójcik, V. Kukula-Koch, K. Kowalik, M. Polak-Berecka, A. Waśko, Evolution of the anticholinesterase, antioxidant, and anti-inflammatory activity of *Epilobium angustifolium L.* infusion during in vitro digestion, J. Funct.Foods 85 (2021) 104645, https://doi.org/10.1016/j.jff.2021.104645.

[51] E. Studzińska-Sroka, A. Majchrzak-Celińska, P. Zalewski, D. Szwajgier, E. Baranowska-Wójcik, B. Kaproń, T. Plech, T. Żarowski, J. Cielecka-Piontek, Lichen-derived compounds and extracts as biologically active substances with anticancer and neuroprotective properties, Pharmaceuticals 14 (2021) 1293, https://doi.org/10.3390/ph14121293.

[52] M. Watanabe, L.B. de Moura Neiva, C.X. da Costa Santos, F.R. Martins Laurindo, M. de Fátima Fernandes Vattimo, Isoflavone and the heme oxygenase system in ischemic acute kidney injury in rats, Food Chem. Toxicol. 45 (2007) 2366–2371.
[53] B. Skóra, T. Piechowiak, K.A. Szychowski, J. Gmiński, Entrapment of silver nanoparticles in L-α-phosphatidylcholine/cholesterol-based liposomes mitigates the oxidative stress in human keratinocyte (HaCaT) cells, Eur. J. Pharm. Biopharm. 166 (2021) 163–174, https://doi.org/10.1016/j.ejpb.2021.06.006.
[54] K.A. Szychowski, B. Skóra, The elastin-derived peptide (VGVAPG) activates autophagy in neuroblastoma (SH-SY5Y) cells via peroxisome proliferator-activated receptor gamma (PPARγ), Mol. Cell. Neurosci. 127 (2023) 103902, https://doi.org/10.1016/j.mcn.2023.103902.
[55] P.K. Smith, R.I. Krohn, G.T. Hermanson, A.K. Mallia, F.H. Gartner, M.D. Provenzano, E.K. Fujimoto, N.M. Goeke, B.J. Olson, D.C. Klenk, Measurement of protein using bicinchoninic acid, Anal. Biochem. 150 (1985) 76–85, https://doi.org/10.1016/0003-2697(85)90442-7.
[56] A.D. Becke, Density-functional thermochemistry. III. The role of exact exchange, J. Chem. Phys. 98 (7) (1993) 5648–5652, https://doi.org/10.1063/1.464913.
[57] J.P. Perdew, K. Burke, M. Ernzerhof, Generalized gradient approximation made simple, Phys. Rev. Lett. 77 (1996) 3865–3868, https://doi.org/10.1103/PhysRevLett.77.3865.
[58] J.P. Perdew, K. Burke K, M. Ernzerhof, Generalized gradient approximation made simple-ERRATA, Phys. Rev. Lett. 78 (1997) 1396, https://doi.org/10.1103/PhysRevLett.77.3865.
[59] R. Dennington, T. Keith, J. Millam, GaussView (2009).
[60] A.R. Allouche, A. Gabedit, Graphical user interface for computational chemistry softwares, J. Comput. Chem. 32 (2011) 174–182, https://doi.org/10.1002/jcc.21600.
[61] D.A. Zainuri, I.A. Razak, S. Arshad, Molecular structure, DFT studies and UV–Vis absorption of two new linear fused ring chalcones: (E)-1-(anthracen-9-yl)-3-(2-methoxyphenyl)prop-2-en-1-one and (E)-1-(anthracen-9-yl)-3-(3-fluoro-4-methoxyphenyl)prop-2-en-1-one, Acta Cryst E74 (2018) 1087–1092, https://doi.org/10.1107/S205698901800974X.
[62] A. Vishnu, Adole. DFT calculations on three 2,3-dihydrobenzofuran linked chalcones: structural, HOMO-LUMO and spectroscopic (UV-Vis and IR) interpretation, Vietnam J. Chem. 61 (2) (2023) 147–157, https://doi.org/10.1002/vjch.202100023.
[63] E.F. Pettersen, T.D. Goddard, C.C. Huang, G.S. Couch, D.M. Greenblatt, E.C. Meng, T.E. Ferrin, UCSF Chimera-a visualization system for exploratory research and analysis, J. Comput. Chem. 25 (13) (2004) 1605–1612.
[64] R.A. Laskowski, M.B. Swindells, LigPlot+: multiple ligand–protein interaction diagrams for drug discovery, J. Chem. Inf. Model. 51 (10) (2011) 2778–2786, https://doi.org/10.1021/ci200227u.
[65] A.C. Wallace, R.A. Laskowski, J.M. Thornton, LIGPLOT: a program to generate schematic diagrams of protein-ligand interactions, Protein Eng. 8 (2) (1995) 127–134, https://doi.org/10.1093/protein/8.2.127.